



# Lawrence Berkeley Laboratory

UNIVERSITY OF CALIFORNIA

## Materials & Chemical Sciences Division

Submitted to Journal of Electrochemistry

### Mass Transport to Cylindrical Electrodes Rotating in Suspensions of Inert Microspheres

D.W. Gibbons, R.H. Muller, and C.W. Tobias

December 1990



1 LOAN COPY 1  
1 Circulates 1  
1 for 2 weeks 1

Bldg. 50 Library.

LBL-29846

## **DISCLAIMER**

This document was prepared as an account of work sponsored by the United States Government. While this document is believed to contain correct information, neither the United States Government nor any agency thereof, nor the Regents of the University of California, nor any of their employees, makes any warranty, express or implied, or assumes any legal responsibility for the accuracy, completeness, or usefulness of any information, apparatus, product, or process disclosed, or represents that its use would not infringe privately owned rights. Reference herein to any specific commercial product, process, or service by its trade name, trademark, manufacturer, or otherwise, does not necessarily constitute or imply its endorsement, recommendation, or favoring by the United States Government or any agency thereof, or the Regents of the University of California. The views and opinions of authors expressed herein do not necessarily state or reflect those of the United States Government or any agency thereof or the Regents of the University of California.

**Mass Transport to Cylindrical Electrodes  
Rotating in Suspensions of  
Inert Microspheres**

D. W. Gibbons, R. H. Muller, and C. W. Tobias

Department of Chemical Engineering and  
Chemical Sciences Division of Lawrence Berkeley Laboratory  
University of California  
Berkeley, CA 94720

December 1990

This work was supported by the Office of Energy Research, Office of Basic Energy Sciences, Materials Science Division of the U.S. Department of Energy, under Contract No. DE-AC03-76SF00098.

## Mass Transport to Cylindrical Electrodes Rotating in Suspensions of Inert Microspheres

D. W. Gibbons\*, R. H. Muller, and C. W. Tobias

*Department of Chemical Engineering and  
Chemical Sciences Division of Lawrence Berkeley Laboratory  
University of California  
Berkeley, CA 94720*

### ABSTRACT

Mass transfer enhancement produced by the addition of inert microspheres was investigated on a rotating cylinder electrode operating in the turbulent regime. The effects of rotation speed, rotor radius, particle size, solids volume fraction, and particle density on the rate of mass transfer were determined by limiting current measurements for ferricyanide ion reduction. In comparison to transport rates observed with clear electrolytes, up to two and a half fold higher limiting currents were obtained in concentrated suspensions containing 5 - 80  $\mu\text{m}$  diameter microspheres with densities ranging from 0.7 to 2.1  $\text{g}/\text{cm}^3$ . Transport enhancement is attributed to the microconvective eddies produced by particle rotation in the shear field adjacent to the spinning electrode, and to the increased shear rate caused by the formation of a particle-free wall layer. Experimental data could be correlated in the form:

$$Sh = \alpha Re^\beta Sc^{1/3}$$

where  $Sh$ ,  $Re$ ,  $Sc$  are the Sherwood, Reynolds, and Schmidt numbers, respectively, and  $\alpha$  and  $\beta$  are empirical functions of solids volume fraction determined from transport rate measurements.

Addition of appreciable volume fractions of inert particles to the electrolyte results in significant improvements of production capacity when the latter is limited by transport rates. The use of suspended particles to achieve a given increase in limiting current density is shown to require far less power than simply increasing electrode rotation speed to enhance mass transport.

Suspended solid particles in moving electrolytes are known to cause a reduction of the mass transfer boundary layer thickness at the electrode surface; mass transfer rates may be increased by a factor of three or more depending on such variables as shear rate, volume fraction solids ( $\Phi$ ), and particle size. Electrochemical studies of mass transport enhancement in suspensions utilizing rotational geometries are summarized in Table 1 (1-10). The rotating disk electrode (RDE) experimental studies are quite complete; the effect of particle size, particle density, electrode size, and electrode rotation rate have been determined. However, only limited investigations have been reported concerning the transport effects of particulates on rotating cylindrical

---

\* Present Address: ELTECH Research Corporation, 625 East Street, Fairport Harbor, Ohio 44077

electrodes (RCE), which have greater technological utility.

Microconvection caused by the rotation of particles near the electrode surface is generally considered to be the key mechanism responsible for transport enhancement. Since an isolated, suspended sphere rotates with an angular velocity ( $\omega$ ) equal to one-half the local shear rate (11), ie.  $\omega = \gamma/2$ , several investigators have correlated their transport data in terms of a Peclet number based on the bulk shear rate ( $\gamma$ ) and particle radius ( $a$ ). Some of these correlations for suspensions undergoing laminar flow are summarized in Table 2 (12-15, 7, 9). The ratio of the effective diffusivity  $D^*$  to the molecular diffusivity  $D$  is the relevant mass transfer Sherwood number.

An additional mechanism may contribute to transport enhancement. Particle migration in the vicinity of the walls, even for well-mixed suspensions, results in the formation of a particle depleted liquid layer often called a *particle-free wall layer*. Poiseuille noticed such an effect in 1836 in his studies of blood flow in which he mentioned a corpuscle-free region near the walls of a capillary (16). The thickness of this layer is estimated to be on the order of 1 to 2 particle radii (17, 18, 19, 20). The formation of such a layer increases the transport to the wall by increasing the local shear rate. The presence of particle-free wall layers in turbulent flow has not yet been experimentally verified, but it seems reasonable to believe that such a layer exists.

Based on these earlier studies of particle-wall interactions, we may construct a picture of the possible flow field near a plate undergoing simple shear flow shown in Figure 1. The shear field creates a net torque on the spheres which produces the counterclockwise rotation, and a slip layer of thickness  $\delta_s$  occurs at the bottom moving plate such that the shear rate (slope of the velocity profile) near the wall increases. Figure 1 is a highly idealized picture of the wall region in a flowing suspension; particles in a dense suspension may be unable to rotate freely because of particle-particle interactions and collisions between the particles may force them into the slip layer.

### Proposed Correlation of Transport Enhancement

Because a solution of the convective diffusion equation in the turbulent flow field of the

rotating cylinder system is not possible, a correlation of the data based on the idealized picture of the wall region presented in Figure 1 will be proposed. Most successful correlations of forced convection mass transport data in single phase fluids have the form:

$$Sh = \alpha Re^\beta Sc^\sigma \quad [1]$$

where  $\alpha$ ,  $\beta$ ,  $\sigma$  are constants. For laminar flow the Reynolds and Schmidt numbers are often combined to yield the Peclet number ( $Pe = ReSc$ ) to decrease the number of adjustable parameters; such a practice was observed with the correlations presented in Table 2. For turbulent flow, however,  $Re$  and  $Sc$  are usually kept separate. Selman and Tobias have reviewed mass transfer correlations established by limiting current measurements and the vast majority of the results for turbulent flow include a  $Sc^{1/3}$  dependence (21). This functionality will be assumed here because the Schmidt number was not varied for a given volume fraction during these experiments.

The Sherwood number is defined as the ratio of the total flux to the diffusive flux; for electrode reactions it may be written as

$$Sh = \frac{i_l^* L}{nFD_i C_b} \quad [2]$$

where  $i_l^*$  is the limiting current measured in suspension,  $L$  is a characteristic length,  $n$  is the number of electrons transferred,  $F$  is Faraday's constant (96,487 *Coulombs/equiv*),  $D_i$  is the reactant diffusion coefficient, and  $C_b$  is the bulk reactant concentration. The Reynolds number is

$$Re = \frac{vL}{\nu^*} \quad [3]$$

where  $v$  is a characteristic velocity. Assuming the effective viscosity,  $\mu^*$ , is independent of particle size (22, 23), the effective kinematic viscosity ( $\nu^*$ ) is calculated from the Thomas correlation (24),

$$\frac{\mu^*}{\mu} = 1 + 2.5\Phi + 10.05\Phi^2 + .00273e^{16.6\Phi} \quad [4]$$

and the following expression for the effective density

$$\rho^* = \Phi\rho_s + (1 - \Phi)\rho_f \quad [5]$$

where  $\rho_s$  and  $\rho_f$  are the densities of the pure solid and fluid phases, respectively.

As illustrated in Table 2, the characteristic velocity ( $v$ ) for transport in suspensions is not the bulk fluid velocity, but rather the rotational velocity of the spheres. This rotational velocity is related to the local shear rate;  $\omega = \gamma/2$  for an isolated sphere in a simple shear field. In fact, both the slip layer and microconvective enhancement mechanisms are proportional to the wall shear rate,  $\gamma$ . Therefore it seems reasonable to write

$$v = \gamma a$$

The shear rate ( $\gamma = \partial v_\theta / \partial r$ ) must be calculated from experimental torque measurements because an analytical expression for the shear rate is not available for the turbulent flow field of the rotating cylinder system. Both Wendt (25) and Theodorsen and Regier (26) performed such experiments, but the latter investigators considered larger gap widths more appropriate here. Theodorsen and Regier correlated their results in terms of the friction factor,  $f$ , as follows

$$\frac{0.1737}{\sqrt{f/2}} = -0.2979 + \log(Re_{r_i} \sqrt{f/2}) \quad [6]$$

where  $Re_{r_i} = 2\Omega r_i^2 / \nu$ . For  $1000 \leq Re_{r_i} \leq 100,000$  Eisenberg et. al. (27) showed that Equation [6] could be approximated as

$$f/2 = .0794 Re_{r_i}^{-3} \quad [7]$$

The friction factor is defined by the force ( $F$ ) exerted on the cylinder by the fluid

$$F = 2\pi r_i l \tau_w = 2\pi r_i l \left[ \frac{1}{2} \rho (\Omega r_i)^2 \right] f \quad [8]$$

where  $\tau_w$  is the wall shear stress and  $l$  is the length of the cylinder. Combining Equations [7] and [8] yields an expression for the shear rate at the surface of the spinning electrode

$$\gamma = \frac{\tau_w}{\mu^*} = \frac{G}{\pi r_i^2 l \mu^*} = \frac{0.0645 r_i^{1.4} \Omega^{1.7}}{v^{*.7}} \quad [9]$$

where  $G$  is the torque exerted on the cylinder by the fluid.

There are three possibilities for the characteristic length,  $L$ , in the rotating cylinder system: the particle radius  $a$ , the gap width ( $r_o - r_i$ ), and the rotor radius ( $r_i$ ). A comparison

between the data and the correlations based on these dimensions must be made to choose the proper length. The previous work concerning mass transport in suspensions reviewed in Table 2 suggests that  $a$ , the particle radius, is the proper length scale. The proposed correlation of mass transport in suspensions undergoing turbulent flow in a rotating cylinder geometry then takes the form

$$Sh = \frac{i_l^* a}{nFD_i C_b} = \alpha(\Phi) Re^{\beta(\Phi)} Sc^{1/3} = \alpha(\Phi) \left[ \frac{a^2 r_i^{1.4} \Omega^{1.7}}{v^* 1.7} \right]^{\beta(\Phi)} \left[ \frac{v^*}{D_i} \right]^{1/3} \quad [10]$$

where  $\alpha(\Phi)$  and  $\beta(\Phi)$  are functions of  $\Phi$  to be determined from the transport data. Note that coefficients of order unity have been neglected in constructing the dimensionless groups.

### Experimental Apparatus and Procedures

The rotating cylinder electrode (RCE) geometry consists of two concentric cylinders; the inner rotor is spun by a variable speed motor to produce a convective flow field while the outer cylinder remains stationary. Homogeneous turbulent flow conditions are achieved at low rotation speeds, and high rates of mass transfer can be obtained in a low volume RCE cell without pumping the solids, an operation which might have damaged the microspheres used in these studies. The shear rate ( $\gamma$ ), and hence the angular velocity ( $\omega$ ) of the particle at the electrode surface, is constant for a given rotation speed in the RCE system. For the RDE, the shear rate is directly proportional to radial position and hence the Peclet number varies across the disk. This distinction between the two geometries is important because the effective diffusivity is a function of the shear rate, and the RCE most easily allows the effect of shear to be isolated.

Despite the geometric simplicity of the RCE, the hydrodynamics of this system are quite complex. The stability of the three distinct flow regimes that may exist can be characterized in terms of the Taylor number (28)

$$Ta = \frac{\Omega r_i (r_o - r_i)^{3/2}}{v r_i^{1/2}} \quad [11]$$

For small values of the gap to rotor radius ratio,  $(r_o - r_i)/r_i$ , the flow regime criteria are

	$Ta < 41.3$	laminar Couette flow with concentric streamlines
41.3	$\leq Ta < 400$	laminar flow with Taylor vortices
	$Ta \geq 400$	turbulent flow

For larger gap to rotor radius ratios, Donnelly (29) and Chandrasekhar (30) reported that the Taylor number required for the first transition increases modestly as  $(r_o - r_i)/r_i$  increases; unfortunately, these authors did not consider the effect of larger gaps on the transition to fully turbulent flow. Based on visual observations, all experiments were conducted in the turbulent flow regime although  $Ta$  was close to 400 for the  $\Phi = 0.40$  suspensions at 250 rpm.

The first extensive study of mass transfer in a RCE system was reported by Eisenberg et al. (ETW) in 1954 (31). For  $835 < Sc < 11,500$  and  $112 < Re_{r_i} < 241,000$ , their results were correlated with an average error of  $\pm 8.3\%$  by the following expression:

$$Sh = \frac{2r_i i_l}{nFD_i C_b} = .0791 Re_{r_i}^{.7} Sc^{.356} = .0791 \left[ \frac{2\Omega r_i^2}{\nu} \right]^{.7} \left[ \frac{\nu}{D_i} \right]^{.356} \quad [12]$$

Numerous investigators have confirmed the validity of Equation [12] (32, 33).

### Microsphere Characterization

The microspheres used in this investigation are detailed in Table 3. The first two entries are solid spheres, while the last three products are hollow, with either thick or thin walls. Each group of particles forms an approximately monodisperse size distribution, and the particles are essentially spherical although each sample contains a few irregular shapes. The Kodak and Anderson Development spheres are used as received from the respective vendors, while the ceramic spheres from Zeelan Industries are subjected to mechanical classification with Tyler sieves.

Particle density is determined by measuring the volume displacement of distilled water by a known weight of particulates. Particle size is determined from scanning electron micrographs taken of representative samples. The diameter,  $d_i$ , of at least 75 particles from each micrograph is measured with a caliper and a volume weighted average diameter,  $\bar{2a}$ , and standard deviation,  $\sigma$ , are calculated according to the following formulae:

$$\bar{2a} = \frac{\sum_i \left(\frac{\pi}{6} d_i^3\right) d_i}{\sum_i \left(\frac{\pi}{6} d_i^3\right)} = \frac{\sum_i d_i^4}{\sum_i d_i^3} \quad [13]$$

$$\sigma = \left[ \frac{\sum_i d_i^3 (d_i - \bar{2a})^2}{\sum_i d_i^3} \right]^{1/2} \quad [14]$$

Based on the previous work reviewed in Tables 1 and 2, it appears that *particle volume fraction* is more important than number density. Therefore, the volume weighted average is considered to be the best measure of particle size. As a practical matter, both measures are nearly identical as can be seen in Table 3 indicating that the samples are nearly monodisperse.

All microspheres are typically used three times. At the end of each experiment, the particles are separated from the electrolyte by vacuum filtration using a Buchner funnel and Whatman #50 filter papers, washed thoroughly with distilled water, and dried at 80°C for 24 hours.

### The Rotating Cylinder Cell

Three different Nickel 200 cylinders with diameters of 1.03, 1.91, and 2.53 *cm* serve as the inner rotating electrode. Each electrode is 13.90 *cm* long and the corresponding electrochemically active areas are 45.00, 83.41, and 110.61 *cm*<sup>2</sup>. An outer cylinder, also composed of Nickel 200, serves as the counter-electrode; it has an internal diameter of 4.80 *cm* and a length of 15.5 *cm*. A 0.6 *cm* gap in the outer electrode allows one to visually observe the fluid flow in the cell. Total cell volumes are 366, 335, and 302 *cm*<sup>3</sup> for the small, medium, and large electrodes. A 0.5 *mm* diameter Nickel 200 wire enclosed in a Luggin capillary acts as the reference electrode. The capillary tip is located in the 0.6 *cm* gap of the outer cylinder and positioned flush with the electrode surface to minimize possible flow disturbances.

Limiting current measurements are conducted in a three-piece, jacketed Lucite cell which contains the concentric Nickel electrodes; a schematic of the apparatus appears in Figure 2. The cell is equipped with a port for maintaining a nitrogen gas blanket during experiments. Ethylene propylene O-rings (Parker Seal Company) provide leak-proof seals between the various cell components and the moving shaft; electrode rotation rate is determined with a digital tachometer.

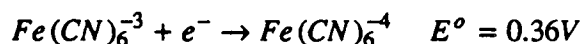
Temperature control is provided by circulating an ethylene glycol - water mixture through

the cell jacket from a 7 liter bath equipped with heaters and a cooler. A proportional controller (Versatherm Model #2156) regulates the dual heaters while the cooler operates continuously. A type K (Chromel-Alumel) thermocouple connected to a digital meter (Doric Trendicator 410A) provides a continuous display of cell temperature to within  $\pm 0.1^\circ\text{C}$ .

A PAR (Princeton Applied Research) Model 371 potentiostat controlled by a PAR Model 175 universal programmer supplies current to the cell. The current is measured as a voltage drop across an  $R = 0.098 \text{ ohm}$  shunt resistor in series with the counter-electrode. Cell voltage and current are monitored by a digital oscilloscope (Nicolet Model 4094) and stored via a data acquisition routine on a microcomputer (IBM PS/2, Model 50z). The current and voltage input signals to the oscilloscope are averaged over a time interval of 0.2s at a constant sampling rate of  $250 \mu\text{s}/\text{pt}$  utilizing the "point average" switch on the Nicolet unit. This averaging is necessary because of small current fluctuations in the presence of suspended solids.

#### *Limiting Current Measurement Procedure*

The ferricyanide/ferrocyanide redox couple is chosen to characterize the rate of mass transport in this system. The kinetics of the redox reaction are quite fast on a Nickel electrode, and a large excess of sodium hydroxide as the supporting electrolyte eliminates the contribution of ionic migration to the limiting current. Specifically, the transport limited current density on the inner rotating cylinder is measured for the reduction of ferricyanide to ferrocyanide (34)



The procedure for making limiting current measurements is described below:

- (1) Prepare one liter of electrolyte with the following composition: 2.00 M NaOH, 0.100 M  $\text{K}_4\text{Fe}(\text{CN})_6$ , and 0.0200 M  $\text{K}_3\text{Fe}(\text{CN})_6$ . The composition of these solutions is periodically checked by standard methods of volumetric analysis (35, 36).
- (2) Polish inner cylinder electrode on lathe at 500 rpm with 1200 FEPA grit sandpaper and then 4-6  $\mu\text{m}$  diamond paste (Kay Industrial Diamond Corp.) using Buehler polishing oil as a lubricant. Electrode is then washed with soap and water, acetone, methanol, and distilled water.
- (3) Sparge electrolyte with  $\text{N}_2$  for 30 minutes in an amber bottle to remove dissolved oxygen.
- (4) Evolve  $\text{H}_2$  on the inner cylinder in 2 M NaOH at 500 rpm for 5 minutes to obtain a clean, reproducible surface. This procedure is performed in a separate pretreatment vessel.
- (5) Weigh desired quantity of microspheres and add to the requisite volume of electrolyte; mix well on a magnetic stir plate and transfer solution to main cell. Mix well at 2000 rpm.
- (6) When cell temperature has stabilized at  $25 \pm 1.0^\circ\text{C}$ , ramp potential (versus Nickel wire

reference electrode) of the rotating cathode from 0.0 V to -1.1 V at 5 mv/s and record the limiting current at various rotation speeds from 250 to 4000 rpm.

## Experimental Results

### *Limiting Currents in Absence of Suspended Solids*

A graph of typical  $i$ - $V$  polarization curves for various electrode rotation speeds is shown in Figure 3. The limiting current density,  $i_l$ , is the value of the current corresponding to the long, flat plateau exhibited at each rotation speed. The limiting currents obtained without solids agreed closely with those predicted from the ETW correlation, Equation [12], but the following expression represented our  $\Phi = 0.0$  data more accurately ( $\pm 5.5\%$ ) for  $1000 < Re_{r_i} < 90,000$

$$Sh = \frac{2r_i i_l}{nFD_i C_b} = .128(Re_{r_i})^{.671} Sc^{1/3} = .128 \left[ \frac{2r_i^2 \Omega}{\nu} \right]^{.671} \left[ \frac{\nu}{D_i} \right]^{1/3} \quad [15]$$

Values of the ferricyanide diffusivity, electrolyte density, and viscosity were calculated with the empirical equations by Gordon et. al. (37) and Boeffard (38). The values of  $D_i$ ,  $\rho$ , and  $\mu$  are  $4.88 \times 10^{-6} \text{ cm}^2/\text{s}$ ,  $1.104 \text{ g/cm}^3$ , and  $0.01457 \text{ g/(cm}\cdot\text{s)}$  for the 2.00 M NaOH, 0.100 M  $K_4Fe(CN)_6$ , and 0.0200 M  $K_3Fe(CN)_6$  solutions employed in all experiments reported here.

Limiting currents obtained with each electrode on at least 4 different days using 4 different solutions were also correlated separately. Figure 4 shows the results of the linear least-squares regression of these data for the  $D = 1.91 \text{ cm}$  electrode. The power dependence of  $i_l$  on  $\Omega$  was 0.66, 0.69, and 0.71 for the small, medium, and large electrodes, respectively. These regressed values of  $i_l$  shall be referred to as the  $\Phi = 0.0$  case in the remainder of this report.

### *Limiting Currents in Suspensions of Microspheres*

*Effect of Microsphere Density*-- Limiting current densities were measured in suspensions of neutrally buoyant polystyrene spheres ( $\bar{2}a = 46.3 \mu\text{m}$ ,  $\rho_s = 1.08 \text{ g/cm}^3$ ) and  $SiO_2$ - $Al_2O_3$  ceramic spheres ( $\bar{2}a = 46.6 \mu\text{m}$ ,  $\rho_s = 2.14 \text{ g/cm}^3$ ) more dense than the electrolyte to investigate the effect of particle density. Typical results are illustrated in Figure 5. The addition of a cationic surfactant, sodium dodecyl sulfate (SDS), was necessary to wet the polystyrene spheres which tended to agglomerate in the pure electrolyte. Limiting currents with surfactant present, but in the absence of solids, were on the average 9% lower than those for ferricyanide reduction

without surfactant. Therefore, the polystyrene data were expected to be slightly lower than the values for the heavy spheres, provided particle density has no effect on the rate of mass transport in these suspensions. However, as shown in Figure 5, the effect of density is quite dramatic.

*The ceramic spheres were more effective transport promoters at and below 1000 rpm, but produced lower enhancements than the neutrally buoyant particles at high rotation speeds.* Centrifugal forces most likely caused this phenomenon since the dense particles would be pushed away from the electrode surface in a centrifugal force field, and therefore produce less mixing. Other experimental observations support this proposition. The data obtained with the  $D = 1.03 \text{ cm}$  Ni electrode produced a straight line on a  $\log i_l^*$  versus  $\log \Omega$  plot, consistent with the foregoing hypothesis because the force exerted on a particle in a centrifugal force field is proportional to  $r_i, \Omega^2, a^3$  (39). Furthermore, the  $46.6 \mu\text{m}$  heavy ceramic spheres showed more bending in the  $\log i_l^*$  versus  $\log \Omega$  graphs than the  $25.0 \mu\text{m}$  spheres of the same density.

If spheres denser than the electrolyte were pushed away from the electrode surface, spheres less dense than the electrolyte should be pushed toward it. Therefore, *light particles are expected to be efficient transport promoters at relatively low volume fractions* (compared to the heavy beads) *because the local solids concentration near the spinning electrode should be much higher than in the bulk* as a result of the centrifugal force field. It is also likely that high bulk volume fractions of solids produce electrode blockage. Indeed, such phenomena are reflected in Figure 6 where  $i_l^*$  is plotted versus  $\Omega$  for suspensions of  $\text{SiO}_2\text{-Al}_2\text{O}_3$  spheres ( $\bar{2a} = 79.9 \mu\text{m}$  and  $\rho_s = 0.697 \text{ g/cm}^3$ )<sup>†</sup>. At  $\Phi = 10\%$  these solids produced substantial increases in the limiting current densities; in fact, these values were larger than the  $\Phi = 40\%$  case.

*Effect of Electrode Rotation Speed--* The effect of electrode rotation speed on the limiting current depends on particle density as described earlier. For suspensions of the neutrally buoy-

---

<sup>†</sup>Unfortunately, light beads with  $\bar{2a} = 46 \mu\text{m}$  could not be obtained for comparison with the dense and neutrally buoyant spheres.

ant spheres, the current density was proportional to  $\Omega^{.75}$ . In Figure 5, a straight line can easily be drawn through these ( $\rho_s = 1.08 \text{ g/cm}^3$ ) points with a slightly larger slope than the  $\Phi = 0.0$  line. In contrast, the slope of the data observed in suspensions of heavier spheres is variable.

In general, the relative enhancement ( $i_l^*/i_l$ ), which is related to  $D^*/D$ , is a function of particle size, volume fraction, electrode rotation speed, and particle density. For the neutrally buoyant spheres,  $i_l^*/i_l$  generally increases as  $\Omega$  increases; this trend is shown in Figure 7. Figure 8 illustrates the complex behavior of the enhancement factor for the heavy microspheres. For  $\Phi = 0.2$  and  $0.3$ ,  $i_l^*/i_l$  decreases as  $\Omega$  increases. For  $\Phi = 0.40$ ,  $i_l^*/i_l$  increased up to 2000 rpm and then decreased while  $i_l^*/i_l$  varied very little with  $\Omega$  at  $\Phi = 0.10$ . An explanation for all of this complex behavior cannot be offered without further investigations concerning the turbulent hydrodynamics of suspensions in the RCE geometry.

*Effect of Solids Volume Fraction--* The limiting current density does not vary monotonically with solids volume fraction; in fact, a plateau exists in plots of  $i_l^*$  versus  $\Phi$  for all particle diameters and electrode sizes studied. As illustrated in Figures 7 and 8,  $i_l^*$  increases with  $\Phi$  up to 20 or 30% solids and then levels off. With the exception of the light ( $\rho_s = 0.697 \text{ g/cm}^3$ ) spheres, very little enhancement is produced at  $\Phi = 0.10$  for the suspensions investigated. A plateau (or maximum) in the limiting current density versus solids volume fraction probably resulted from decreased cross-sectional area for mass flux, the high solution viscosity and consequent reduction of turbulence. Recall Equation [4], the effective viscosity of a suspension increases rapidly for  $\Phi > 0.25$ , and  $i_l^*$  decreases as  $\mu^*$  increases. Since the distance between adjacent sphere surfaces is less than  $a$  for  $\Phi > 0.20$  assuming hexagonal packing (40), the spheres may have been close enough to inhibit the turbulent eddy motion otherwise responsible for transport enhancement.

*Effect of Rotor Radius--* The  $\Phi = 0.0$  data indicated that the limiting current density is proportional to  $r_i^{.34}$  for the RCE operated in the turbulent flow regime without solids present, see Equation [15]. Figure 9 displays the effect of rotor radius on the rate of mass transfer upon the addition of inert polystyrene spheres. As  $r_i$  increases the limiting current increases as expected

because the shear rate increases, but the power dependence of  $i_l^*$  on  $r_i$  increased from 0.34 to 0.55. The exact power depends slightly on particle size and volume fraction.

*Effect of Particle Size*-- The effect of particle size was examined with  $\text{SiO}_2\text{-Al}_2\text{O}_3$  spheres of two different diameters from Zeelan Industries ( $\rho_s = 2.14 \text{ g/cm}^3$ ). Typical results for all electrode sizes are depicted in Figure 10 for the 2.53 cm diameter Ni cathode comparing 25.0 and 46.6  $\mu\text{m}$  diameter spheres. The larger particles were more efficient transport promoters below 2500 rpm for all volume fractions and electrodes studied. However, the degree of enhancement above 2500 rpm decreases, and in a few cases, the 25  $\mu\text{m}$  spheres produce higher limiting currents. As described earlier, such behavior may be caused by the centrifugal force field which pushes the larger particles farther away from the electrode surface than the smaller ones. Finally, the dependence of transport rate on particle radius is relatively weak, approximately  $a^{1/5}$ .

The effect of particle size was also investigated with polymer microspheres of nearly the same density ( $1.08 \text{ g/cm}^3$  and  $1.20 \text{ g/cm}^3$ ), but an order of magnitude difference in size, 46.3  $\mu\text{m}$  versus 4.95  $\mu\text{m}$ . In this case the effect of particle size depended on volume fraction and rotation speed. For  $\Phi = 0.10$ , the smaller spheres yielded larger enhancements, while at  $\Phi = 0.30$ , the larger spheres produced the highest limiting currents. For  $\Phi = 0.20$ , the 4.95  $\mu\text{m}$  particles produced larger enhancements below 1500 rpm only. Furthermore, the rate of mass transport displayed a very weak dependence on  $a$ , changing the particle size by an order of magnitude for the same  $\Phi$  and  $\Omega$  changed  $i_l^*$  by 30% or less.

#### A Correlation of the Data

The data were correlated according to Equation [10]. For each limiting current measurement,  $Sh/Sc^{1/3}$  was calculated and plotted logarithmically versus the particle Reynolds number defined earlier;  $\alpha$  and  $\beta$  were then obtained by a linear least-squares regression of the experimental data. The concentration of the pure suspending fluid was used to construct the Sherwood number, ie.  $C_b = 0.0200 \text{ M Fe(CN)}_6^{-3}$  regardless of  $\Phi$ . These plots are shown in Figures 11 through 14 for the 25.0 and 46.6  $\mu\text{m}$  spheres ( $\rho_s = 2.14 \text{ g/cm}^3$ ) with the three different

electrode diameters. Figure 15 contains a summary of the regressed lines for different values of  $\Phi$ . The values of  $\alpha$  and  $\beta$  are summarized in Table 4 for the heavy microspheres and Table 5 for the neutrally buoyant polystyrene spheres. For the dense spheres, the coefficient  $\alpha$  is given by  $\alpha = 0.14\Phi^{64}$  for all  $\Phi$  and, ignoring the  $\Phi = 0.40$  data in Table 4,  $\beta$  is found to be independent of  $\Phi$  to a first approximation. An average value of  $\beta = 0.43$  represents the dense sphere data well for  $0.10 \leq \Phi \leq 0.30$ . A value of  $\beta = 0.45$  represents the neutrally buoyant data well for all  $\Phi$ . The small ( $\bar{2a} = 4.95 \mu m$ ) spheres were not included in that correlation because of the limited number of experiments performed, the extremely large difference in particle radius, and the slightly different particle densities.

The correlation represents the data reasonably well except for the  $\Phi = 0.40$  case with the dense ceramic spheres as illustrated in Figure 14. For  $Re > 10$  in that figure, the Sherwood number displayed almost no dependence on  $Re$ . Somehow, the turbulent mixing was inhibited. This effect is probably caused by particle inertia because the neutrally buoyant spheres do not show the same behavior at  $\Phi = 0.40$ . According to viscosity measurements reported by Andersen et. al. (41), suspensions of glass spheres ( $\rho_s = 2.49 g/cm^3$ ) in the size range of 5-60  $\mu m$  behave as Newtonian fluids at least for volume fractions up to 40%. Thus, non-Newtonian behavior does not appear to be a plausible explanation for the failure of the correlation at  $\Phi = 0.40$ .

As mentioned earlier, there are 3 possibilities for the characteristic length,  $L$ , in this system:  $a$ ,  $r_o - r_i$ , and  $r_i$ . A correlation of the transport data for the ceramic spheres based on  $r_i$  simply does not work. Although it is slightly better for  $\Phi = .40$ , the correlation based on the gap width produces poorer results for  $\Phi = 0.10, 0.20,$  and  $0.30$  than the one based on  $a$ . Therefore, the gap width does not appear to be the proper length scale, either. For mass transfer in single phase fluids, the gap dimension is unimportant provided  $(r_o - r_i)/r_i$  is larger than 0.10 (42, 43). The experiments described in this report considered gap to rotor radius ratios of 0.90 to 3.66.

### *Experimental Error and Reproducibility*

Several sources of experimental error exist, ranging from electrolyte composition and solids volume fraction to microsphere degradation by mechanical abrasion. Upon completion of a series of experiments, an SEM micrograph of the  $SiO_2-Al_2O_3$  spheres revealed that a small number had been fractured; this may have affected the results by altering the shape and size distribution of a sample. Rather than quantify the effects of all possible error sources, the experimental reproducibility was examined. Limiting current measurements conducted on different days with various solids loadings agreed within  $\pm 7\%$ . Without solids, the reproducibility was  $\pm 4\%$ .

### **Discussion**

Transport augmentation obtained by the addition of solids is surprising based on the bulk properties of suspensions. The addition of solids decreases the effective concentration of reactant, increases the effective viscosity, and decreases the cross-sectional area available for mass flux. Such behavior should decrease the rate of mass transfer in suspensions; however, the experimentally measured limiting currents indicate that *the addition of solids significantly increases the rate of mass transport*.

Such increases may be caused by the microconvective eddies created by particle rotation in the shear field adjacent to the spinning electrode and the formation of a particle-free wall layer. A dimensionless correlation based on a *particle rotation model*, Equation [10], agrees reasonably well with the experimental data. However, the size dependence of  $i_l^*$  predicted from the correlation, given the values of  $\beta$  in Tables 4 and 5, does not agree with the experimental data. The correlation predicts a limiting current density proportional to  $a^{-1}$  while the data show a proportionality of  $a^{1/5}$ . Because of this discrepancy, use of the correlation beyond the range of variables investigated in this study is not recommended. More experimentation is necessary to fully determine the effect of microsphere radius on mass transport in this system.

As a linear least-squares regression of dimensionless groups, the correlation is a

compromise between various variables, the  $a$  dependence is the weakest and is therefore masked by the  $\Omega$  and  $r_i$  functionalities. Physically, the discrepancy between Equation [10] and the experimental data may be the result of particle collisions and subsequent direct interaction with the boundary layer, two phenomena not considered in the formulation of the correlation. Goldsmith and Karino reported enhanced diffusivity in flowing suspensions of red blood cells and attributed (based on photographic evidence) the transport enhancement to the erratic radial displacements in the paths of the cells (44). The authors claimed this migration mechanism was proportional to shear rate also. Thus, it appears that particle rotation is not necessary for transport enhancement.

A simplex (multidimensional parameter optimization) fit of the dense sphere data to the following relation:  $i_l^* = \alpha_1 \Omega^{\alpha_2} r_i^{\alpha_3} a^{\alpha_4} \text{ mA/cm}^2$  was also performed where the  $\alpha_i$ 's are adjustable parameters. The results are tabulated in Table 6; the average error between the data and this simplex result is smaller than that observed with Equation [10], but the number of parameters has been doubled.

#### *Comparison with Results of Previous Work*

The largest value of the enhancement factor,  $i_l^*/i_l$ , obtained in this work is 2.7 at 4000 rpm with the 46.3  $\mu\text{m}$  diameter neutrally buoyant spheres for a volume fraction of 0.30 and an electrode diameter of 1.91 cm. The magnitude of this increase agrees well with the other entries in Table 1 for both laminar and turbulent flow.

There are no published correlations for mass transport in suspensions employing an RCE geometry to compare with the one presented in this report. Of the published work reviewed in Table 1, only Kim examined different sizes and densities of microspheres with the rotating cylinder electrode (8). Our data agree qualitatively with his results, but a quantitative comparison is not possible because of the widely different microsphere densities employed in the respective investigations. For 30 and 68  $\mu\text{m}$  spheres less dense than the electrolyte, he found that the larger spheres produced the highest limiting currents. Also, Kim reported decreased relative enhancement with beads denser than the electrolyte, ie.  $i_l^*/i_l$  decreased as  $\Omega$  increased

above 1000 rpm; this is consistent with our results for the heavy spheres,  $\rho_s = 2.14 \text{ g/cm}^3$ .

The particle size dependence of the limiting current on an RCE for spheres more dense than the electrolyte differs from the RDE studies in which the limiting current was inversely proportional to particle size in the 25-100  $\mu\text{m}$  size range (2, 3, 7). In contrast, the limiting current density is proportional to particle radius for the RCE in the same size range. Perhaps the smaller spheres, which are closer together for a given  $\Phi$  than the larger particles, dampen the otherwise effective turbulent eddies. Similar to our results with the RCE, a plateau in the limiting current density above  $\Phi = 0.30$  was reported by Roha and Doh with the RDE system (2, 3). Other investigators mentioned in Table 1 examined lower volume fractions or simply did not present their data in a way that elucidated the dependence on solids volume fraction.

#### *Power Requirements and Energy Efficiency*

The addition of suspended particles to a fluid increases both the rate of mass transfer and viscous dissipation. The energy efficiency of an electrochemical process operating with suspended particles reflects a balance between the benefits of faster production, versus increased agitation/pumping costs and ohmic losses. Suppose one desires to plate a metal on an RCE, adding solids shortens deposition time by increasing the rate of transport, but requires more energy to spin the cylinder. The power ( $P$ ) required to drive a rotating cylinder equals the product of the torque,  $G$ , and the rotation rate:

$$P = G \Omega \quad [16]$$

Substituting Equation [9] for  $G$  written for a single phase fluid, Equation [16] can be written

$$P = 0.0645\pi l \rho^{.7} \mu^{.3} r_i^{3.4} \Omega^{2.7} \quad [17]$$

where  $l$  is the electrode length. Thus, the ratio  $P/P^*$  may be expressed as

$$\frac{P}{P^*} = \left[ \frac{\rho}{\rho^*} \right]^{.7} \left[ \frac{\mu}{\mu^*} \right]^{.3} \quad [18]$$

where  $P^*$  is the power required to rotate the cylinder in a suspension. The quantity  $i_l^*/i_l$  is obtained by dividing Equation [10] by [15] to yield

$$\frac{i_l^*}{i_l} = \frac{\alpha}{0.102} a^{(2\beta - 1)} r_i^{(1.4\beta - .342)} \Omega^{(1.7\beta - .671)} \nu^{.338} (v^*)^{(1/3 - 1.7\beta)} \quad [19]$$

where  $\alpha$  and  $\beta$  are given by Tables 4 and 5.

Combining [18] and [19] yields the agitation energy efficiency,  $i_l^* P / i_l P^*$ , which is plotted in Figure 16 as a function of electrode speed for the neutrally buoyant polystyrene microspheres ( $\rho_s = 1.08 \text{ g/cm}^3$ ,  $\bar{a} = 46.3 \text{ }\mu\text{m}$ ). The values of this ratio are greater than one, suggesting that the use of suspended solids to enhance mass transfer saves agitation energy compared to the process without solids. For the  $\text{SiO}_2\text{-Al}_2\text{O}_3$  spheres that are almost twice as dense as the electrolyte, the agitation energy efficiency is slightly greater than one only for rotation speeds larger than 1000 rpm. *Neutrally buoyant spheres produce transport enhancements equal to or better than denser particles of the same size and less agitation energy is consumed as well.*

The effective conductivity ( $\kappa^*$ ) of a suspension may be estimated by the Bruggeman equation (45), but the additional ohmic loss in volts depends on the actual distance between electrodes.

$$\frac{\kappa^*}{\kappa} = (1 - \Phi)^{3/2} \quad [20]$$

Ultimately, the portion of total energy consumption that ohmic losses comprise determines whether operating with suspended solids requires a smaller or greater energy expenditure.

One can also compare the energy required for achieving a higher limiting current density by rotating the cylinder faster without particles present, given by Equation [17], with that for keeping the speed constant and adding the 46.3  $\mu\text{m}$  polystyrene spheres. Such an analysis is presented in Figure 17; adding solids at 3000 rpm is compared with rotating the cylinder faster without particulates. Clearly, the addition of inert microspheres provides a method of achieving a given increase in the limiting current density that consumes much less power than simply increasing electrode rotation speed to enhance mass transport. Figure 17 reveals that a 100% increase in the limiting current achieved by rotating the cylinder faster requires an order of magnitude more power than the process operating with suspended solids. The "knee" in the solids addition curve, ie. two different values of  $P$  at a given percentage increase in transport rate,

results from the plateau in the  $i_l^*$  versus  $\Phi$  graph. Increasing solids concentration above 0.30 increases viscous dissipation, yet produces smaller limiting current augmentation.

In addition to increasing the rate of mass transport, the presence of suspended solids may improve deposit uniformity and surface texture. Wisdom (46) and Eisner (47) reported that the addition of suspended solids improved the throwing power of plating baths and thereby produced more uniform deposits. Brown and Tomaszewski (48, 49) claimed that fine powders improved deposit quality and produced satin-like electrodeposits. Such results can eliminate expensive post deposition polishing steps.

### Conclusions

The limiting current density increases upon the addition of inert microspheres as (ranked in relative order of importance) electrode rotation speed, solids volume fraction, rotor radius, and particle radius increase. Particle density is especially important in the RCE system because of the nonuniform solids distribution produced by centrifugal forces. For example, the transport enhancement (relative to no solids present) achieved with beads more dense than the electrolyte decreased at high rotation speeds as a result of particle movement away from the electrode surface in the centrifugal force field created by the spinning cylinder. Since neutrally buoyant spheres produce large increases in the rate of mass transfer, it appears that particle inertia is not a major factor in transport enhancement.

A correlation has been developed for calculation of the limiting current on rotating cylinder electrodes in concentrated suspensions containing 10 - 40% (by volume) inert solid particles. Up to  $\Phi = 0.30$  a single exponent on the Reynolds number may be used without sacrificing accuracy to predict the limiting current density within  $\pm 13\%$  in suspensions of dense spheres:

$$Sh = \alpha Re^{.43} Sc^{1/3}$$

where  $\alpha$  is 0.03, 0.046, 0.069 for  $\Phi = 0.1, 0.2, 0.3$ , respectively. Volume fractions over 0.30 are not of great practical interest; there is less enhancement when  $\Phi$  is larger than 0.30, and the viscous dissipation also increases markedly.

The use of suspended solids appears capable of increasing mass transfer rates by a factor of 2 to 3, decreasing energy costs, and improving deposit quality. The ability of inert particles to efficiently reduce mass transfer boundary layer thicknesses in moving electrolytes should also be of interest whenever the reactant substances are poorly soluble, for example in various electroorganic processes.

#### **Acknowledgements**

This work was supported by the Office of Energy Research, Office of Basic Energy Sciences, Materials Science Division of the U.S. Department of Energy, under Contract No. DE-AC03-76SF00098.

## Nomenclature

### Roman Letters

$a$	particle radius ( $cm$ )
$C_b$	concentration in the bulk ( $moles/l$ )
$C_p$	heat capacity ( $ergs/g^{\circ}C$ )
$d_i$	particle diameter ( $cm$ )
$D$	diameter of inner electrode ( $cm$ )
$D_i$	diffusion coefficient ( $cm^2/s$ )
$E^{\circ}$	equilibrium electrode potential at standard conditions ( $volts$ )
$f$	friction factor
$F$	Faraday's constant ( $96,487\ Coulombs/equiv$ )
$G$	torque ( $dyne \cdot cm$ )
$i$	current density ( $mA/cm^2$ )
$i_l$	limiting current density ( $mA/cm^2$ )
$k$	thermal conductivity ( $ergs/m \cdot s \cdot K$ )
$l$	cylinder length ( $cm$ )
$L$	characteristic length ( $cm$ )
$n$	number of electrons transferred
$P$	Power ( $watts$ )
$Pe$	Peclet number
$r_i$	inner cylinder radius ( $cm$ )
$r_o$	outer cylinder radius ( $cm$ )
$R$	disk electrode radius ( $cm$ )
$Re$	Reynolds number
$Re_{r_i}$	Reynolds number based on $r_i$ ( $2\Omega r_i^2/\nu$ )
$Sc$	Schmidt number ( $\nu/D$ )
$Sh$	Sherwood number ( $i_l L/nFDC_b$ )
$v$	velocity ( $cm/s$ )

### Greek Letters

$\alpha$	empirical coefficient, Eq. [10]
$\beta$	empirical coefficient, Eq. [10]
$\delta_s$	particle free wall layer thickness ( $cm$ )
$\delta_m$	mass transfer boundary layer thickness ( $cm$ )
$\kappa$	ionic conductivity ( $ohm^{-1}cm^{-1}$ )
$\mu$	viscosity ( $g/cm \cdot s$ )
$\nu$	kinematic viscosity ( $cm^2/s$ )
$\omega$	angular rotation speed of particles ( $s^{-1}$ )

$\Omega$	angular rotation speed of cylindrical or disk electrode ( $s^{-1}$ )
$\Phi$	volume fraction of solids
$\gamma$	shear rate ( $s^{-1}$ )
$\pi$	3.14159....
$\rho$	density ( $g/cm^3$ )
$\sigma$	volume weighted standard deviation
$\tau_w$	wall shear stress ( $dyne/cm^2$ )

#### Superscripts

\* suspension property

#### Subscripts

$f$	fluid phase
$n$	population (number) weighted quantity
$s$	solid phase

## References

1. G.C. Pini and P.L. DeAnna, *Electrochimica Acta*, **22**, 1423, (1977).
2. David J. Roha, M.S. Thesis, Department of Chemical Engineering, University of California, Berkeley, Lawrence Berkeley Laboratory LBL-12737, (1981).
3. Dong-Sup Doh, *Hwahak Konghak*, **21**, 235, (1983).
3. D.P. Barkey, Ph.D. Thesis, Department of Chemical Engineering, University of California, Berkeley, Lawrence Berkeley Laboratory LBL-23880, (1987).
5. M. de Ficquelmont-Loizos, L. Tamisier, A. Caprani, *J. Electrochem. Soc.*, **135**, 626, (1988).
6. A. Caprani, M. de Ficquelmont-Loizos, L. Tamisier, P. Peronneau, *J. Electrochem. Soc.*, **135**, 635, (1988).
7. P.K. Andersen, R.H. Muller, C.W. Tobias, *J. Electrochem. Soc.*, **136**, 390, (1989).
8. L.H. Kim, R.H. Muller, C.W. Tobias, Lawrence Berkeley Laboratory LBL-27473, (1989).
9. Y.M. Bashir and J.D. Goddard, *AIChE J.*, **36**, 387, (1990).
10. P.J. Sonneveld, W. Visscher, E. Barendrecht, *J. Appl. Electrochem.*, **20**, 563, (1990).
11. H. Lamb, *Hydrodynamics*, Dover, New York, 1945.
12. L.G. Leal, *Chem. Eng. Commun.*, **1**, 21, (1973).
13. Avinoam Nir and Andreas Acrivos, *J. Fluid Mech.*, **78**, 33, (1976).
14. C.W. Sohn and M.M. Chen, *J. Heat Transfer*, **103**, 47, (1981).
15. Y.C. Chung and L.G. Leal, *Int. J. Multiphase Flow*, **8**, 605, (1982).
16. J.L.M. Poiseuille, *Ann. Sci. Nat.*, **5**, 111, (1836).
17. Vladimir Vand, *J. Phys. and Colloid. Chem.*, **52**, 277, (1948).
18. A. Karnis, H.L. Goldsmith, S.G. Mason, *Can. J. Chem. Eng.*, **44**, 181, (1966).
19. S. Einav, S.L. Lee, *Int. J. Multiphase. Flow*, **1**, 73, (1973).
20. Robert W. Watkins, Channing R. Robertson, Andreas Acrivos, *Int. J. Heat and Mass Transfer*, **19**, 693, (1976).
21. J.R. Selman and C.W. Tobias, *Adv. in Chem. Eng.*, **10**, 211, (1978).
22. G.F. Eveson, *The Rheology of Disperse Systems*, ed. by C.C. Mill, Pergamon, London, 61, (1959).
23. D.J. Jeffrey, Andreas Acrivos, *AIChE J.*, **22**, 417, (1976).
24. David G. Thomas, *J. Colloid. Sci.*, **20**, 267, (1965).

25. V.F. Wendt, *Ingen.-Arch.*, **4**, 577, (1933).
26. Theodore Theodorsen and Arthur Regier, *Nat. Advisory Comm. Aeronaut.*, Report # 793, (1945).
27. M. Eisenberg, C.W. Tobias, C.R. Wilke, *Chem. Eng. Prog. Symp. Ser.*, **51**, 1, (1955).
28. Hermann Schlichting, *Boundary Layer Theory*, McGraw-Hill Book Company, New York, 526, (1979).
29. R.J. Donnelly, *Proc. Roy. Soc., Series A*, **246**, 312, (1958).
30. S. Chandrasekhar, *Proc. Roy. Soc., Series A*, **246**, 301, (1958).
31. M. Eisenberg, C.W. Tobias, C.R. Wilke, *J. Electrochem. Soc.*, **101**, 306, (1954).
32. D.R. Gabe, *J. Appl. Electrochem.*, **4**, 91, (1974).
33. D.R. Gabe and F.C. Walsh, *J. Appl. Electrochem.*, **13**, 3, (1983).
34. *Lange's Handbook of Chemistry*, ed. by John A. Dean, Twelfth Edition, McGraw-Hill, New York, p. 6-5, (1979).
35. F. Sutton, *A Systematic Handbook of Volumetric Analysis*, Butterworths, London, pp. 331, 335-336, (1955).
36. I.M. Kolthoff, R. Belcher, *Volumetric Analysis, Vol. III*, Interscience Publishers, Inc., New York, p. 344, (1957).
37. S.L. Gordon, J.S. Newman, C.W. Tobias, *Berichte der Bunsengesellschaft für physikalische Chemie*, **70**, 414, (1966).
38. A. Boeffard, M.S. Thesis, Department of Chemical Engineering, University of California, Berkeley, Lawrence Radiation Laboratory UCRL-16624, 26, (1966).
39. M.M. Denn, *Process Fluid Mechanics*, Prentice-Hall, Englewood Cliffs, NJ, 56, (1980).
40. R.A. Bagnold, *Proc. Roy. Soc. London Ser. A*, **225**, 49, (1954).
41. P.K. Andersen, R.H. Muller, C.W. Tobias, *J. Electrochem. Soc.*, **136**, 390, (1989).
42. M. Eisenberg, C.W. Tobias, C.R. Wilke, *Chem. Eng. Prog. Symp. Ser.*, **51**, 1, (1955).
43. Charles M. Mohr, Ph.D. Thesis, Department of Chemical Engineering, University of California, Berkeley, Lawrence Berkeley Laboratory LBL-3913, pp. 71-88, (1975).
44. H.L. Goldsmith and T. Karino, in *Quantitative Cardiovascular Studies in Clinical and Research Applications of Engineering Principles*, ed. by N.A. Hwang, D.R. Gross, D.J. Patel, University Park Press, Baltimore, 290, (1979).
45. D.A.G. Bruggeman, *Ann. Physik.*, **24**, 636, (1935).
46. N.E. Wisdom, *U.S. # 3,699,015*, (1972).
47. S. Eisner, *U.S. # 3,699,017*, (1972).

48. H. Brown and T.W. Tomaszewski, *U.S. # 3,152,972*, (1964).
49. T.W. Tomaszewski and H. Brown, *U.S. # 3,152,973*, (1964).

## Captions

**Table 1.** Literature review of the use of suspended particles in rotational electrochemical systems. For a homogeneous, single phase fluid  $n = 0.5$  for the RDE and  $n = 0.7$  for the RCE, References (1-10). † nonspherical particles.

**Table 2.** Summary of heat and mass transfer correlations for suspensions of rigid spheres in laminar flow. Unless otherwise specified, microspheres are neutrally buoyant, References (12-15, 7, 9).

**Table 3.** Summary of microsphere characterization results.

**Table 4.** Summary of correlation results,  $Sh = \alpha Re^\beta Sc^{1/3}$ , for the rate of mass transport in suspensions of  $SiO_2-Al_2O_3$  spheres from Zeelan Industries ( $\rho_s = 2.14 \text{ g/cm}^3$ ).  $N$  is the number of data points.

**Table 5.** Summary of correlation results,  $Sh = \alpha Re^\beta Sc^{1/3}$ , for the rate of mass transport in suspensions of polystyrene-2%DVB spheres from Eastman Kodak ( $\rho_s = 1.08 \text{ g/cm}^3$ ).

**Table 6.** Summary of simplex fit results,  $i_l^* = \alpha_1 \Omega^{\alpha_2} r_i^{\alpha_3} a^{\alpha_4} \text{ mA/cm}^2$ , for the rate of mass transfer in suspensions of  $SiO_2-Al_2O_3$  spheres from Zeelan Industries ( $\rho_s = 2.14 \text{ g/cm}^3$ ).

**Figure 1.** A suspension undergoing simple shear flow between two flat plates and the resulting particle free wall layer of thickness  $\delta_s$ . Neglecting particle-particle interactions, each sphere experiences a net torque which causes it to rotate counterclockwise.

**Figure 2.** Schematic of the Lucite rotating cylinder cell, the cooling jacket is not shown.

**Figure 3.** Current-voltage curves obtained in the absence of suspended solids for the reduction of ferricyanide ion at the inner, rotating electrode ( $D = 2.53 \text{ cm}$ ).

**Figure 4.** Linear regression of the limiting current density data,  $i_l$ , obtained with the  $D = 1.91 \text{ cm}$  Ni cathode in the absence of solids. Data taken on four different days with 4 different electrolyte solutions of the same composition are shown.

**Figure 5.** Effect of microsphere density,  $\rho_s$ , on  $i_l^*$  for the  $D = 1.91 \text{ cm}$  Ni cathode. The electrolyte used with neutrally buoyant spheres ( $\rho_s = 1.08 \text{ g/cm}^3$ ,  $\bar{a} = 46.3 \text{ }\mu\text{m}$ ) contained  $0.58 \text{ mM}$  SDS surfactant for wetting purposes. Experiments with the  $SiO_2-Al_2O_3$  ceramic spheres ( $\rho_s = 2.14 \text{ g/cm}^3$ ,  $\bar{a} = 46.6 \text{ }\mu\text{m}$ ) were performed without surfactant.

**Figure 6.** Variation in limiting current density with rotation speed as a function of solids volume fraction measured on the  $D = 1.91 \text{ cm}$  Ni electrode. The suspended particles are hollow,  $SiO_2-Al_2O_3$  spheres with a volume weighted average diameter,  $\bar{a}$ , of  $79.9 \text{ }\mu\text{m}$  and a density of  $0.697 \text{ g/cm}^3$ .

**Figure 7.** Enhancement factor ( $i_l^*/i_l$ ) as a function of volume fraction ( $\Phi$ ) for various electrode rotation speeds in suspensions of neutrally buoyant spheres. Electrode diameter =  $2.53 \text{ cm}$ ,  $\bar{a} = 46.3 \text{ }\mu\text{m}$ ,  $\rho_s = 1.08 \text{ g/cm}^3$ ,  $0.58 \text{ mM}$  SDS surfactant.

**Figure 8.** Enhancement factor ( $i_l^*/i_l$ ) as a function of volume fraction ( $\Phi$ ) for various electrode rotation speeds in suspensions of dense spheres. Electrode diameter =  $2.53 \text{ cm}$ ,  $\bar{a} = 46.6 \text{ }\mu\text{m}$ ,  $\rho_s = 2.14 \text{ g/cm}^3$ .

**Figure 9.** Effect of inner electrode diameter ( $D$ ) on the limiting current density in a RCE

system with neutrally buoyant spheres ( $\bar{2a} = 46.3 \mu\text{m}$ ,  $\rho_s = 1.08 \text{ g/cm}^3$ ,  $0.58 \text{ mM}$  SDS surfactant).

**Figure 10.** Effect of particle size on the limiting current density in suspensions of dense spheres,  $\rho_s = 2.14 \text{ g/cm}^3$ . The results shown are for a Ni electrode  $2.53 \text{ cm}$  in diameter.

**Figure 11.** Correlation of mass transfer data in 10% (by volume) suspensions of dense microspheres,  $\rho_s = 2.14 \text{ g/cm}^3$ . The dimensionless quantities  $Sh$ ,  $Re$ , and  $Sc$  are defined in Equation [10]; the line represents a least-squares fit to the data.

**Figure 12.** Correlation of mass transfer data in 20% (by volume) suspensions of dense microspheres,  $\rho_s = 2.14 \text{ g/cm}^3$ . The dimensionless quantities  $Sh$ ,  $Re$ , and  $Sc$  are defined in Equation [10]; the line represents a least-squares fit to the data.

**Figure 13.** Correlation of mass transfer data in 30% (by volume) suspensions of dense microspheres,  $\rho_s = 2.14 \text{ g/cm}^3$ . The dimensionless quantities  $Sh$ ,  $Re$ , and  $Sc$  are defined in Equation [10]; the line represents a least-squares fit to the data.

**Figure 14.** Correlation of mass transfer data in 40% (by volume) suspensions of dense microspheres,  $\rho_s = 2.14 \text{ g/cm}^3$ . The dimensionless quantities  $Sh$ ,  $Re$ , and  $Sc$  are defined in Equation [10]; the line represents a least-squares fit to the data.

**Figure 15.** Summary of mass transfer correlation results as a function of  $\Phi$  for various sizes of electrodes and microspheres ( $\rho_s = 2.14 \text{ g/cm}^3$ ).  $Sh$ ,  $Re$ , and  $Sc$  are defined in Equation [10]; the lines represent a least-squares fit to the data at each respective volume fraction.

**Figure 16.** Agitation energy efficiency,  $(i_l^* P / i_l P^*)$ , as a function of electrode rotation speed. The quantity plotted along the ordinate is given by combining Equations [18] and [19]; a value greater than one reveals that the increase in limiting current density is proportionally larger than the increased power consumption. Hence, the proposed process would save agitation energy.

**Figure 17.** Agitation power,  $P$ , per unit electrode area required to achieve a given increase in limiting current density. The dotted line represents the power consumed by adding microspheres at  $3000 \text{ rpm}$  to increase the transport rate while the solid line represents rotating the cylinder faster without solids present. Calculation performed for  $D = 2.53 \text{ cm}$  inner, cylindrical electrode and  $46.3 \mu\text{m}$  polystyrene spheres.

Investigator	Geometry	System	Type	Size (μm)	Enhancement ( $i_l^*/i_l$ )	Ω (rpm)	Φ	$i_l^* - \Omega^n$
Pini, DeAnna, 1977	RCE	$I^-/I_3^-$	SiC <sup>†</sup>	40-75	2	1980	.002	$n \approx .75$
Roha, 1981	RDE	$Fe(CN)_6^{-3}/Fe(CN)_6^{-4}$	glass	12.4	3.3	2870	.40	$n > .5$
Doh, 1983	RDE	$Fe(CN)_6^{-3}/Fe(CN)_6^{-4}$	glass	14	3	3000	.32	$n > .5$
Barkey, 1987	RCE	$Cu^{+2}/Cu$	glass	80	1.3	1800	.40	$n = .7$
Caprani et.al., 1988	RDE	$Fe(CN)_6^{-3}/Fe(CN)_6^{-4}$ 60% glycerol	Al <sub>2</sub> O <sub>3</sub> <sup>†</sup>	9.0	2	4900	.20	n variable
Andersen et. al., 1989	RDE	$Fe(CN)_6^{-3}/Fe(CN)_6^{-4}$	glass	9.05	3	3000	.40	$n > .5$
Kim et. al., 1989	RCE	$Fe(CN)_6^{-3}/Fe(CN)_6^{-4}$	glass	80	2.7	1000	.30	n variable
Bashir and Goddard, 1990	RDE	$Fe(CN)_6^{-3}/Fe(CN)_6^{-4}$	polymer	5.6	2.1	1200	.30	$n = .5$
Sonneveld et. al., 1990	RDE	$Fe(CN)_6^{-3}/Fe(CN)_6^{-4}$	SiC <sup>†</sup>	12.2	2.25	3820	.24	$n = .5$

Table 1.

XBL 9011-3796

Investigator	Pe	$\Phi$	Correlation	Pe Definition	Comments
Leal, 1973	$Pe \rightarrow 0$	$\Phi \rightarrow 0$	$\frac{D^*}{D} = 1 + \Phi(-\frac{3}{2} + 3.36Pe^{3/2})$	$Pe = \frac{a^2\gamma}{D}$	theoretical, Couette flow
Nir and Acrivos 1976	$Pe \rightarrow \infty$	$\Phi \rightarrow 0$	$\frac{D^*}{D} = 1 + \alpha\Phi Pe^{1/11}$	$Pe = \frac{a^2\gamma}{D}$	theoretical, Couette flow
Sohn and Chen 1981	$300 < Pe < 2000$	.15, .30	$\frac{k^*}{k} = f(\Phi)Pe^{1/2}$	$Pe = \frac{\rho C_p (2a)^2\gamma}{k}$	cylindrical Couette flow
Chung and Leal 1982	$.01 < Pe < 1.3$	$0 \leq \Phi \leq .25$	$\frac{k^*}{k} = \alpha Pe^\beta$	$Pe = \frac{\rho C_p a^2\gamma}{k}$	cylindrical Couette flow $\alpha, \beta$ are functions of $\Phi$
Andersen, 1989	$15 < Pe_\delta < 5600$	$.05 \leq \Phi \leq .40$	$\frac{D^*}{\kappa D} = e^{-5.86\Phi}(Pe_\delta)^{1.59\Phi}$	$Pe_\delta = \frac{2aR\Omega}{(D^2\nu)^{1/3}}$	RDE, heavy microspheres $\kappa = 1 - 3\Phi/2 + \Phi^2/2$
Bashir and Goddard 1990	$100 < Pe < 10^6$	$.04 \leq \Phi \leq .30$	$\frac{D^*}{D} = 1 + 6\Phi Pe^{.05}$	$Pe = \frac{a^2\gamma}{D}$	RDE

XBL 9011-3797

Table 2.

			Volume Weighted		Population Weighted	
Manufacturer	Material	$\rho$ ( $g/cm^3$ )	$\bar{2a}$ ( $\mu m$ )	$\sigma$ ( $\mu m$ )	$\bar{2a}_n$ ( $\mu m$ )	$\sigma_n$ ( $\mu m$ )
Anderson Development Company	butyl methacrylate/ methyl methacrylate	1.20	4.95	2.14	3.12	1.51
Eastman Kodak	polystyrene-2%DVB	1.08	46.3	4.81	44.6	5.11
Zeelan Industries	$SiO_2-Al_2O_3$	2.14	25.0	3.00	23.1	4.43
Zeelan Industries	$SiO_2-Al_2O_3$	2.14	46.6	3.83	43.1	7.76
Zeelan Industries	$SiO_2-Al_2O_3$	0.697	79.9	5.06	78.4	6.19

Table 3.

$\Phi$	Re	N	$\alpha$	$\beta$	Correlation Coefficient	Average Error
0.10	1.62 - 742	40	0.030	0.43	0.948	$\pm 13.5\%$
0.20	0.993 - 454	39	0.050	0.41	0.948	$\pm 12.0\%$
0.30	0.541 - 247	41	0.065	0.45	0.950	$\pm 13.6\%$
0.40	0.686 - 96.5	38	0.078	0.52	0.743	$\pm 36.8\%$

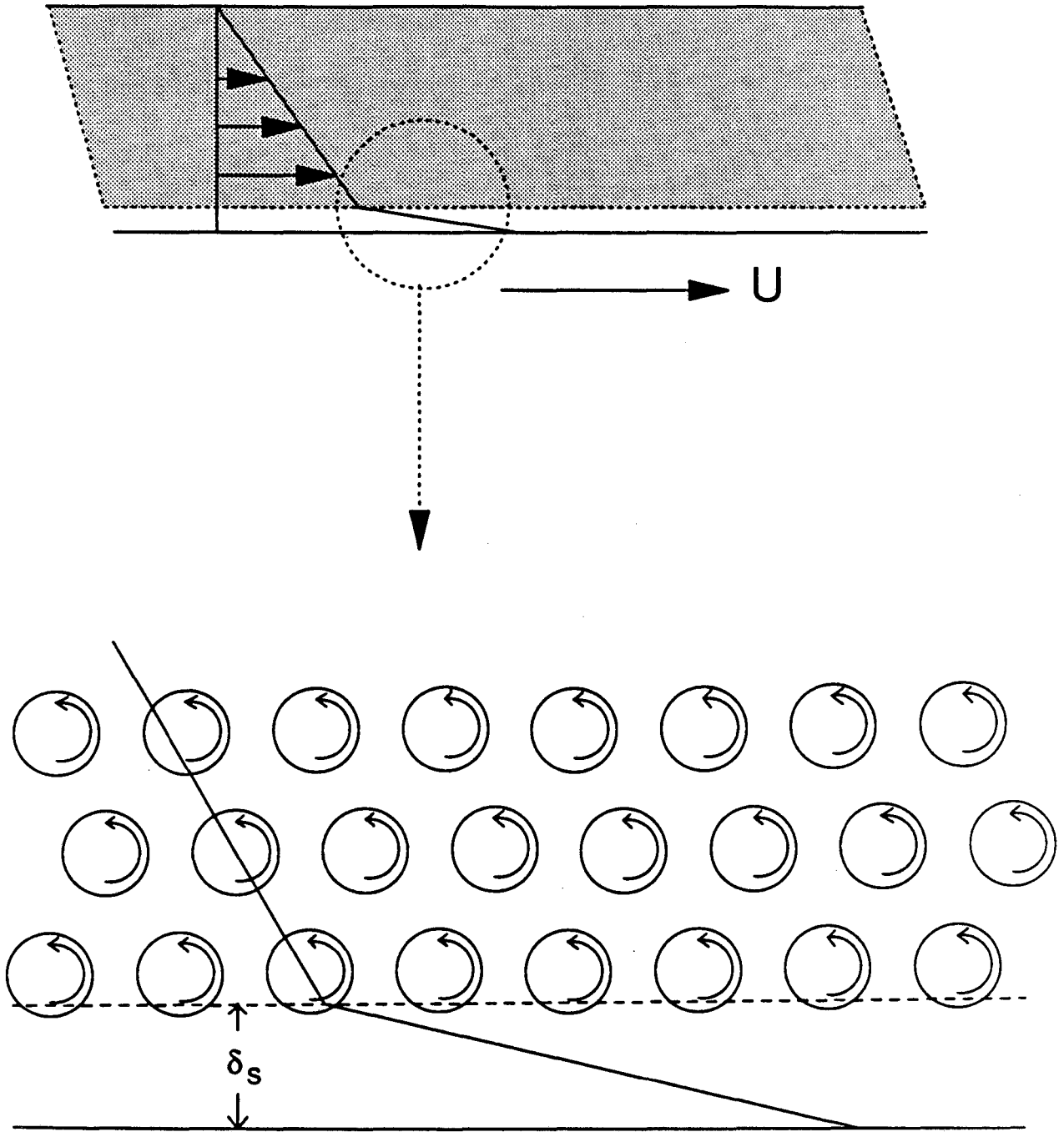
Table 4.

$\Phi$	Re	N	$\alpha$	$\beta$	Correlation Coefficient	Average Error
0.10	2.01 - 627	26	0.041	0.42	0.986	$\pm 6.5\%$
0.20	1.06 - 332	26	0.063	0.45	0.970	$\pm 10.9\%$
0.30	0.507 - 158	26	0.085	0.46	0.987	$\pm 6.7\%$
0.40	0.175 - 54.6	26	0.11	0.45	0.989	$\pm 5.9\%$

Table 5.

$\Phi$	N	$\alpha_1$	$\alpha_2$	$\alpha_3$	$\alpha_4$	Average Error
0.10	26	0.82	0.67	0.46	0.22	$\pm 5.4\%$
0.20	26	0.99	0.65	0.60	0.17	$\pm 8.3\%$
0.30	26	1.18	0.72	0.61	0.22	$\pm 9.8\%$
0.40	26	0.23	0.97	1.19	0.16	$\pm 16.5\%$

Table 6.



XBL 9011-3792

Figure 1

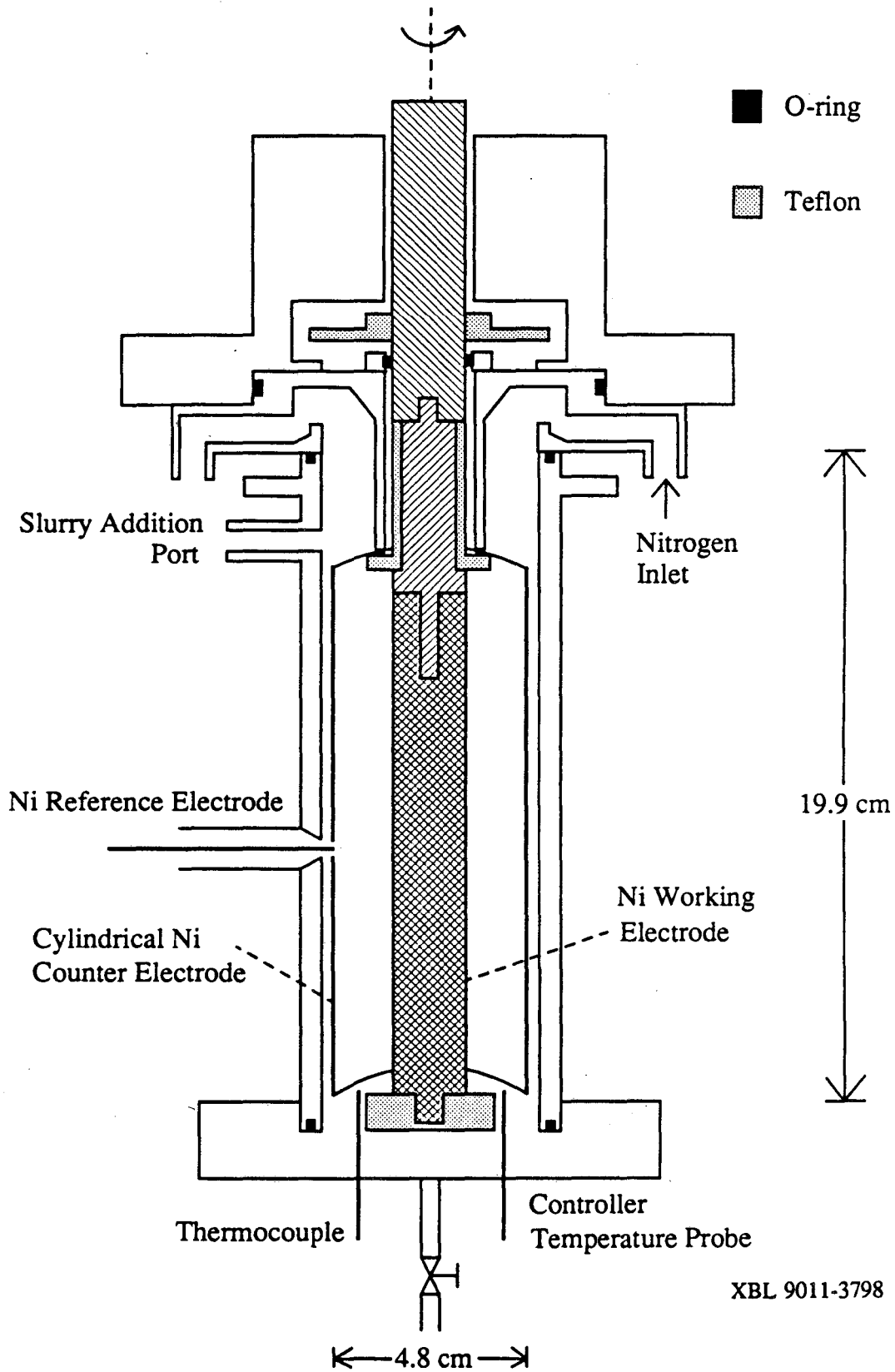
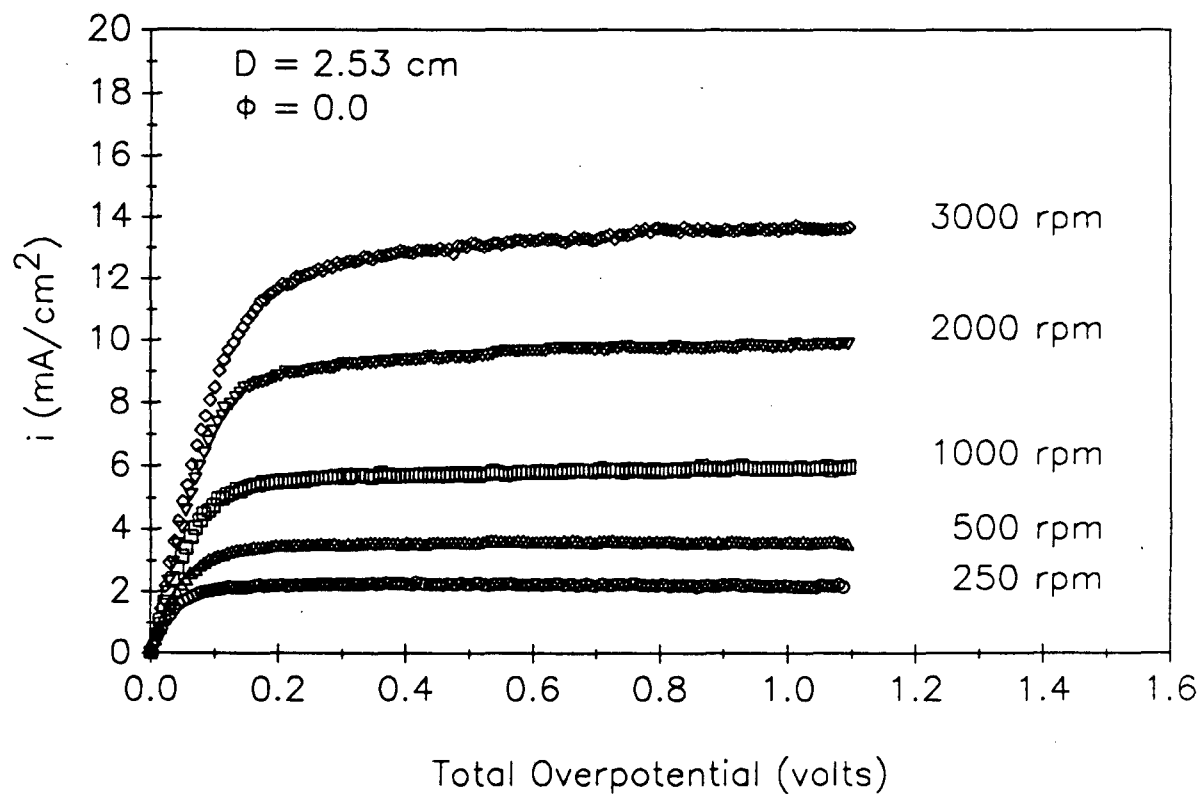
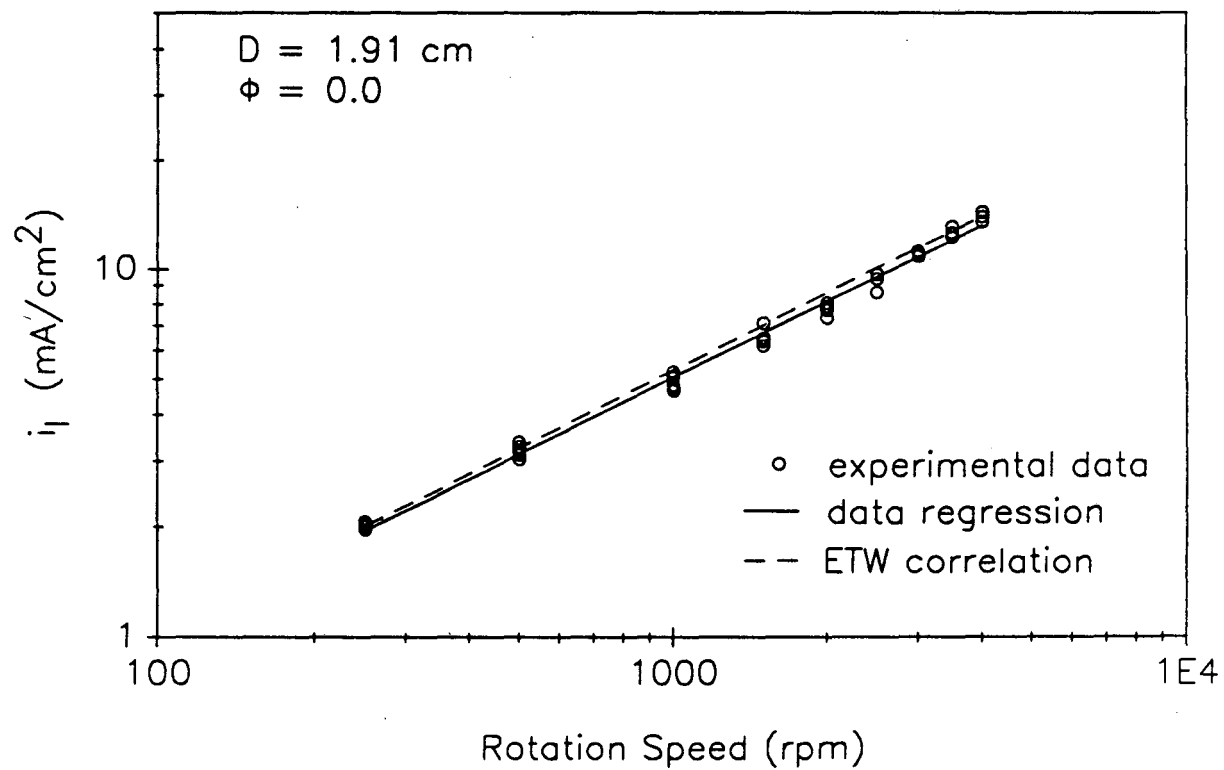


Figure 2



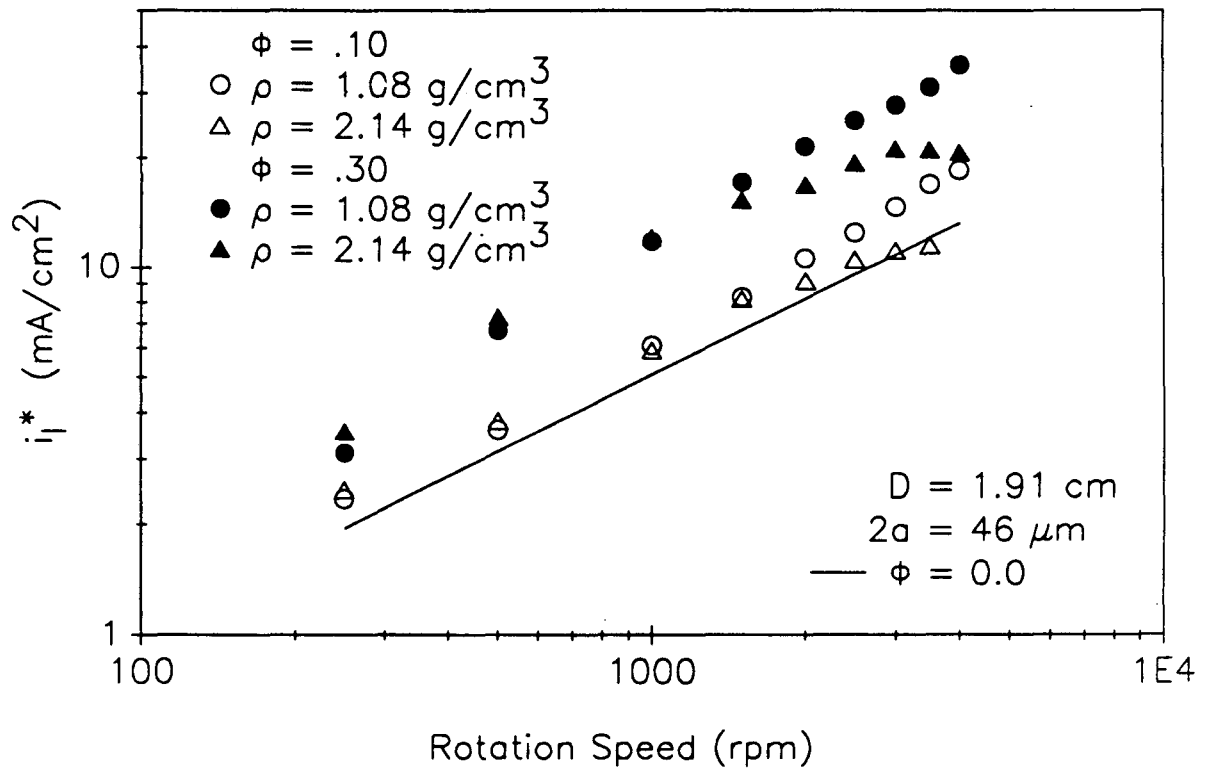
XBL 9011-3801

Figure 3



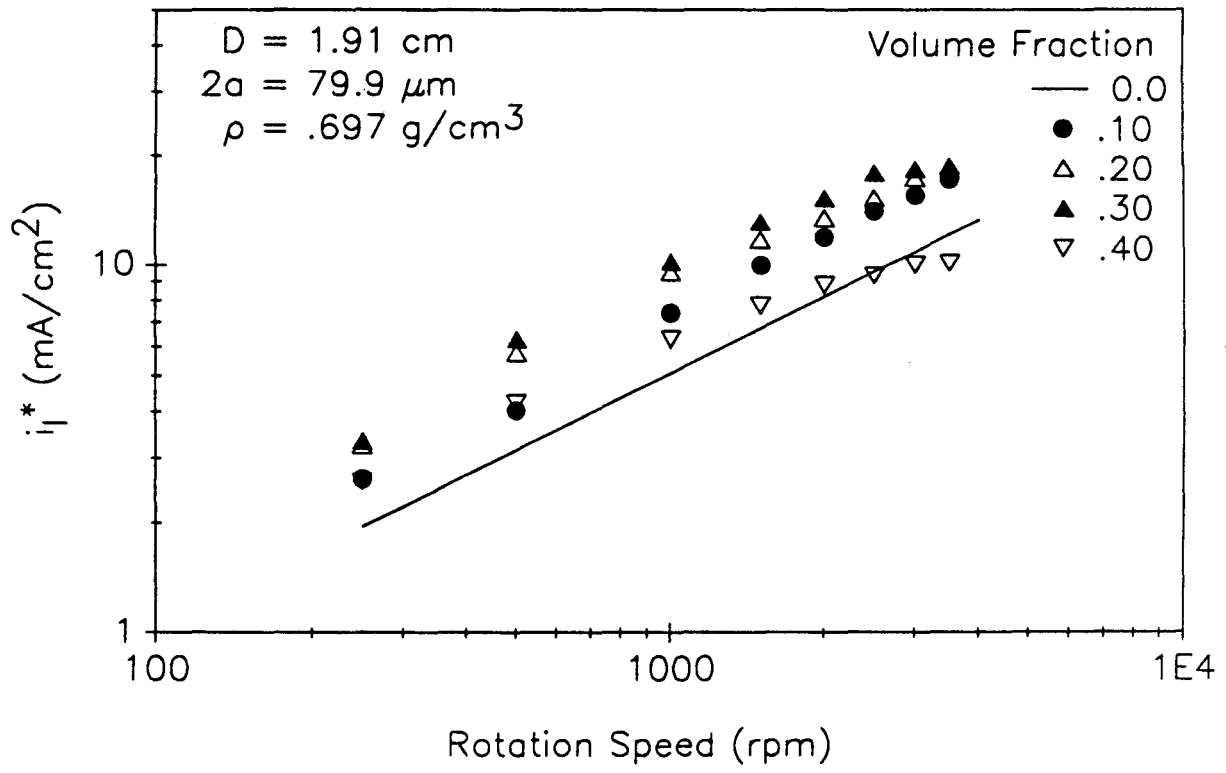
XBL 9011-3802

Figure 4



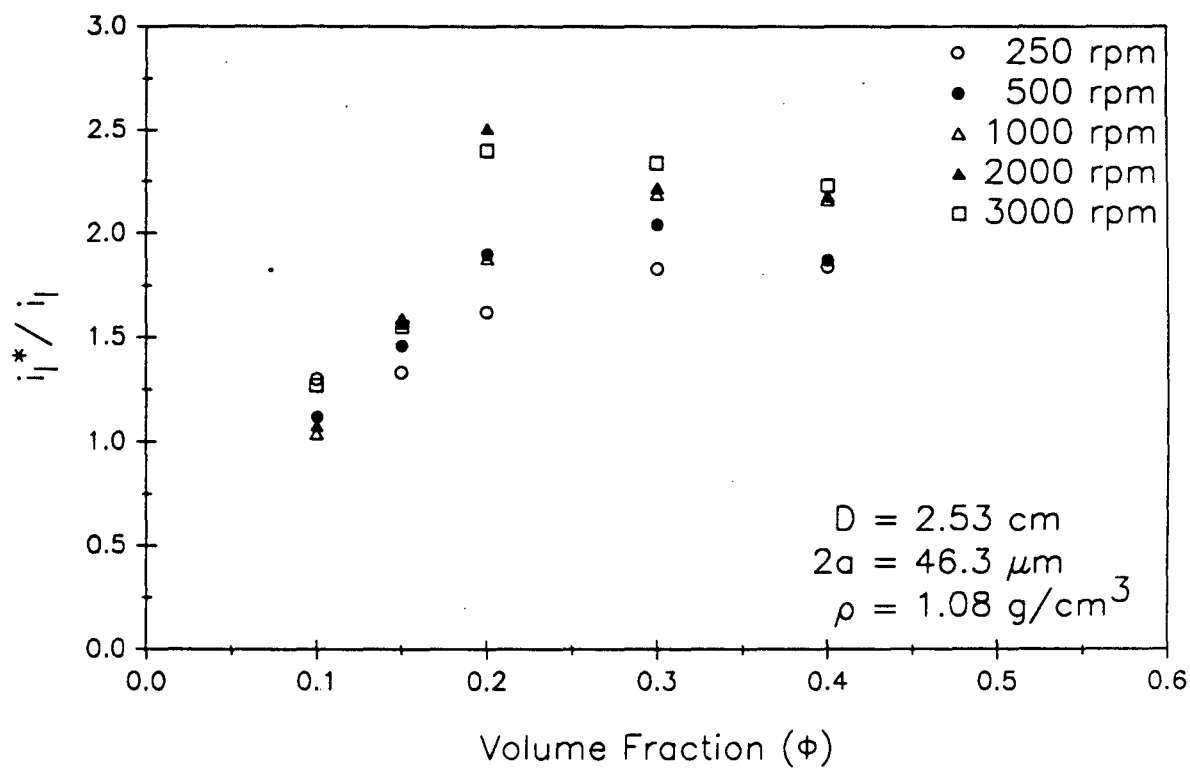
XBL 9011-3803

Figure 5



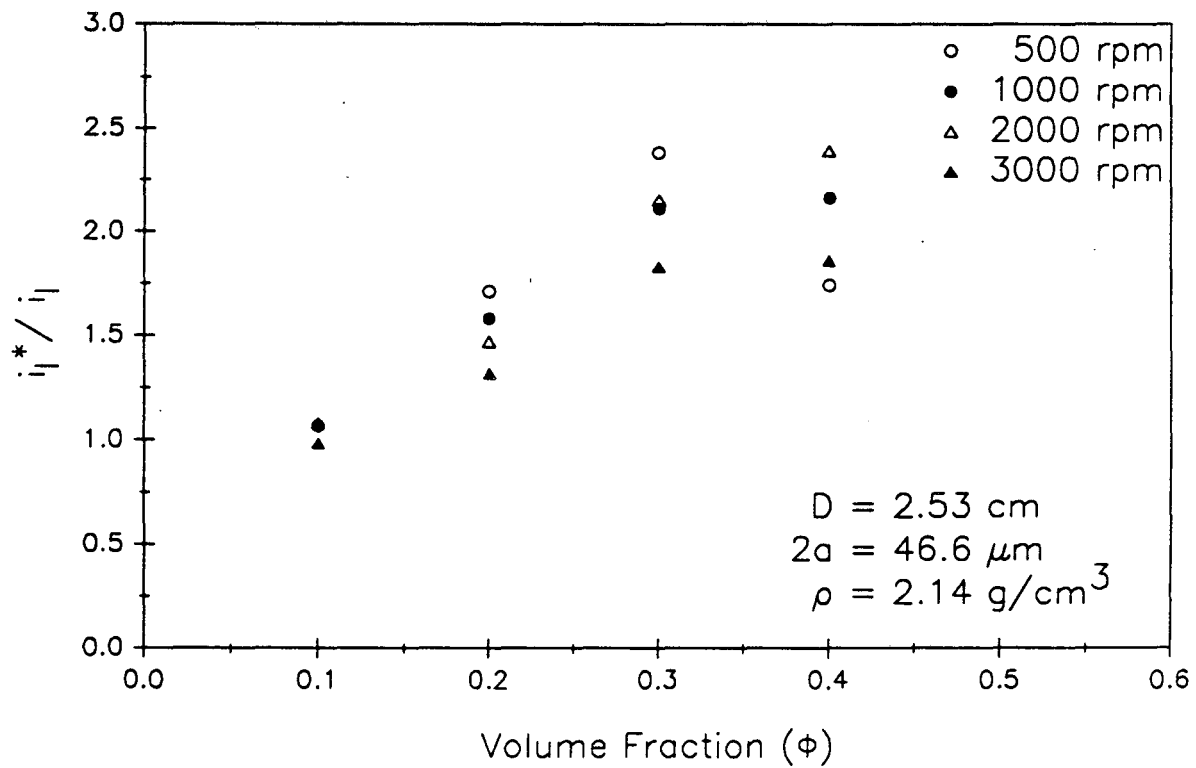
XBL 9011-3804

Figure 6



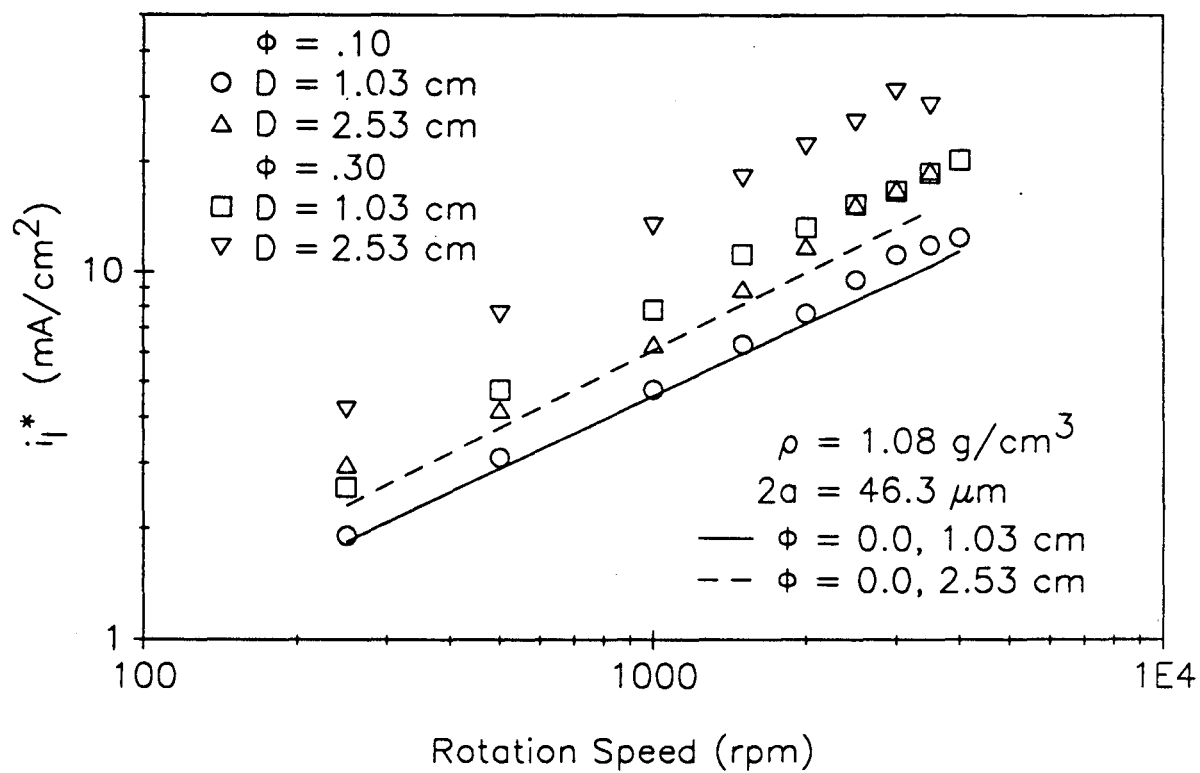
XBL 9011-3805

Figure 7



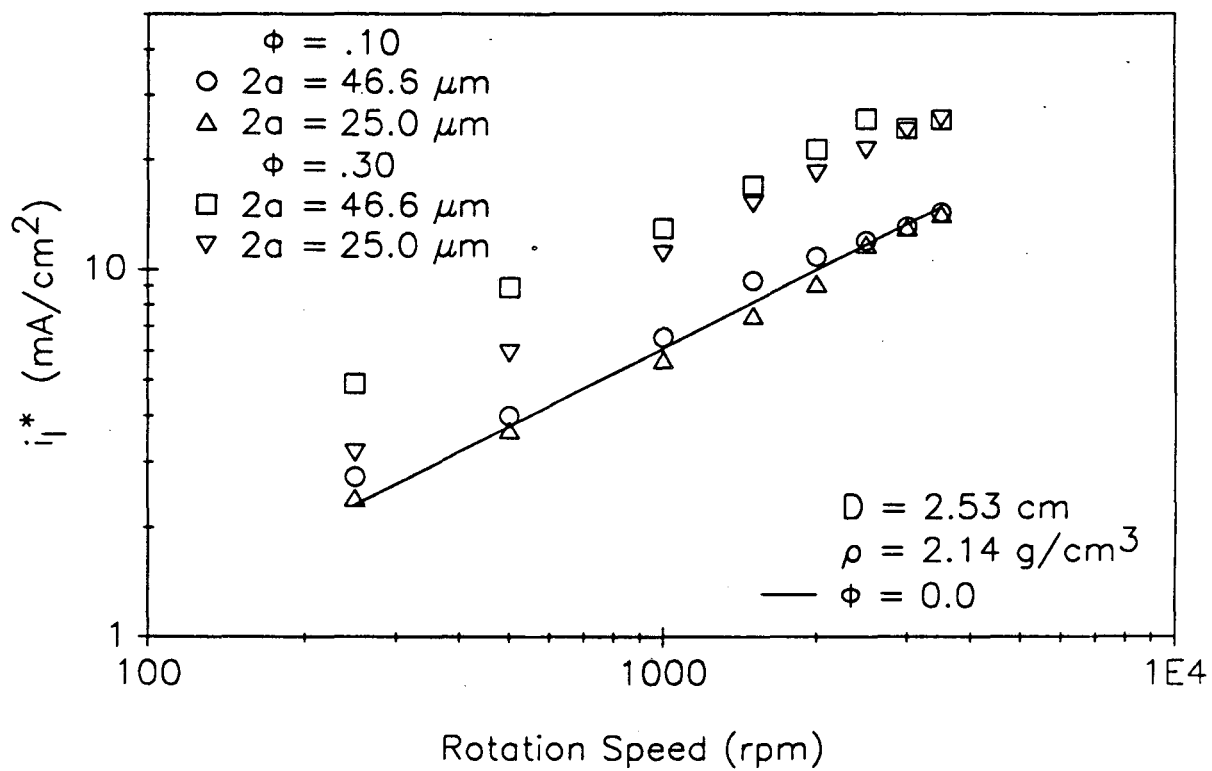
XBL 9011-3806

Figure 8



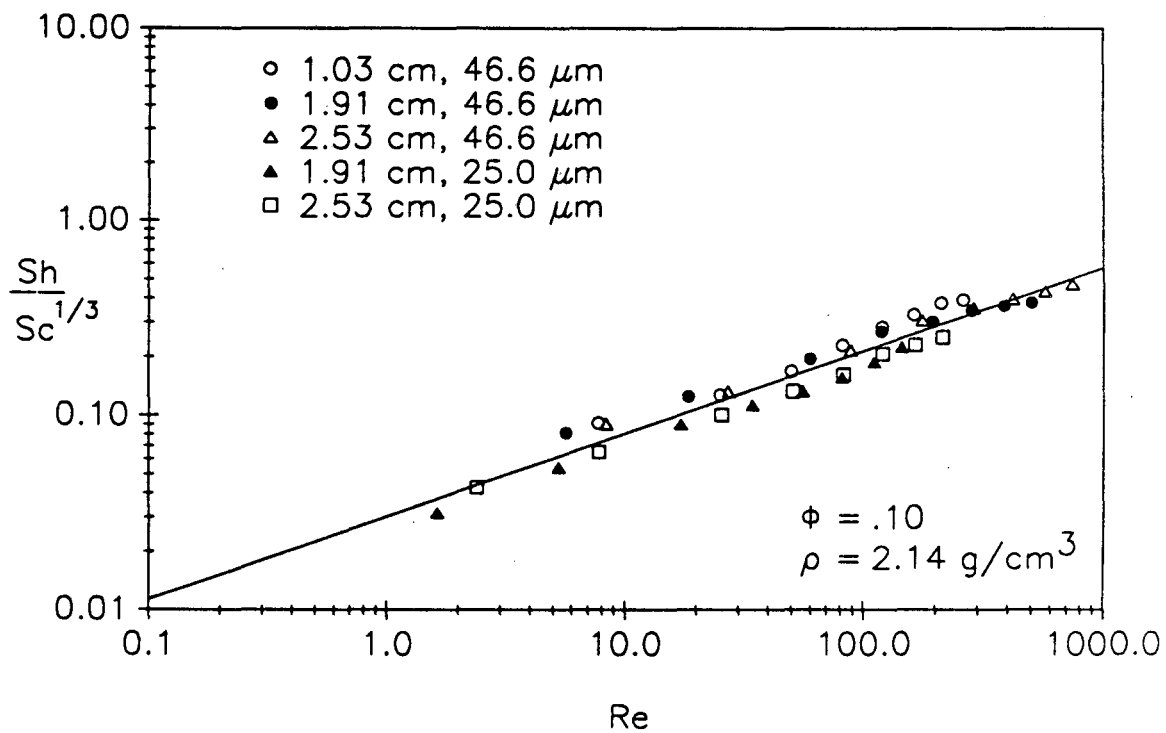
XBL 9011-3807

Figure 9



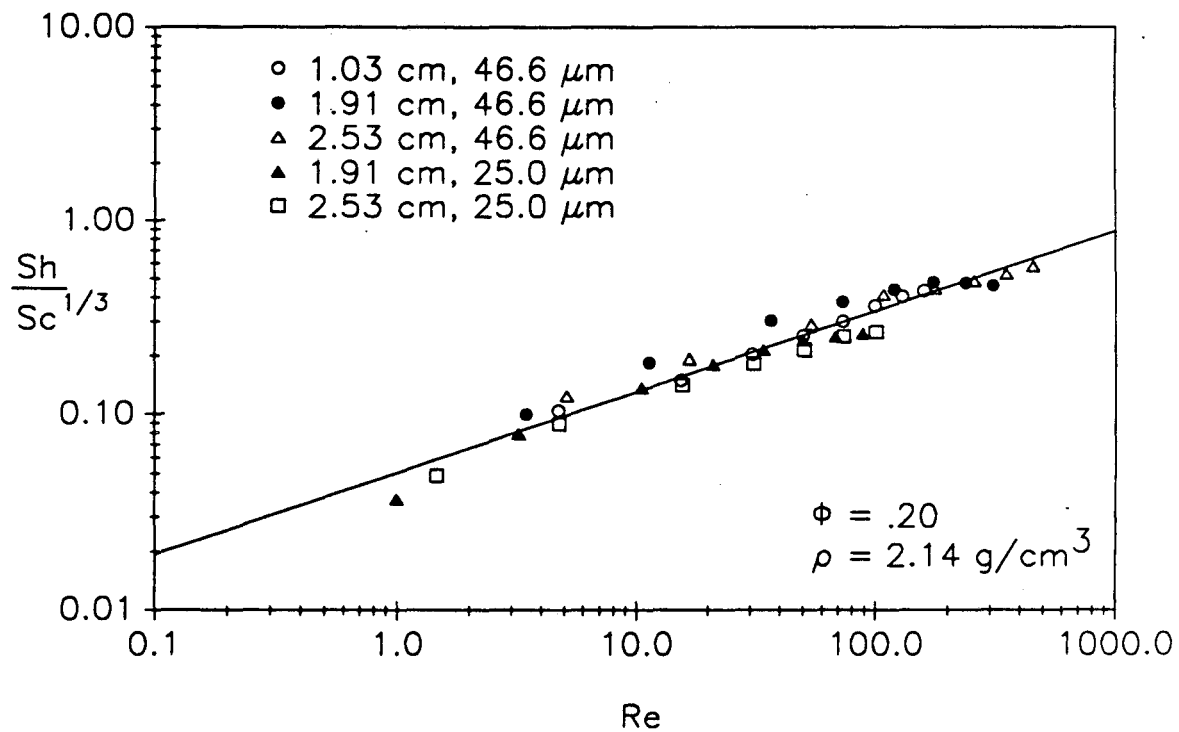
XBL 9011-3808

Figure 10



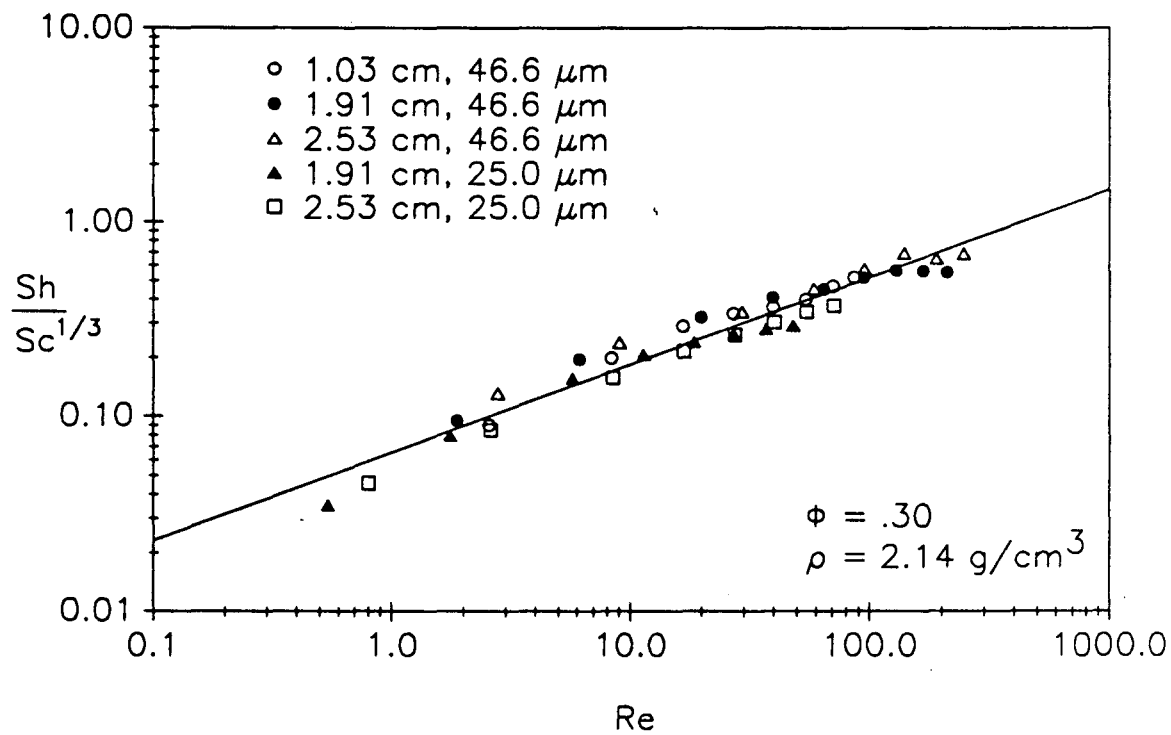
XBL 9011-3809

Figure 11



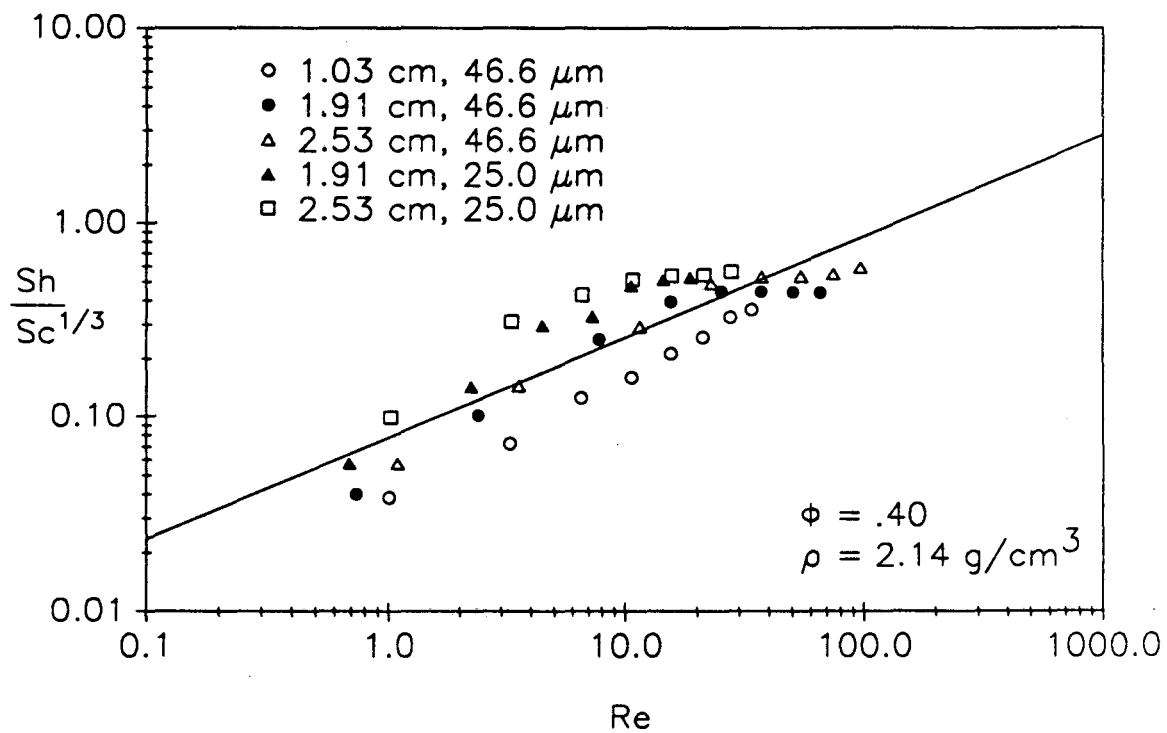
XBL 9011-3810

Figure 12



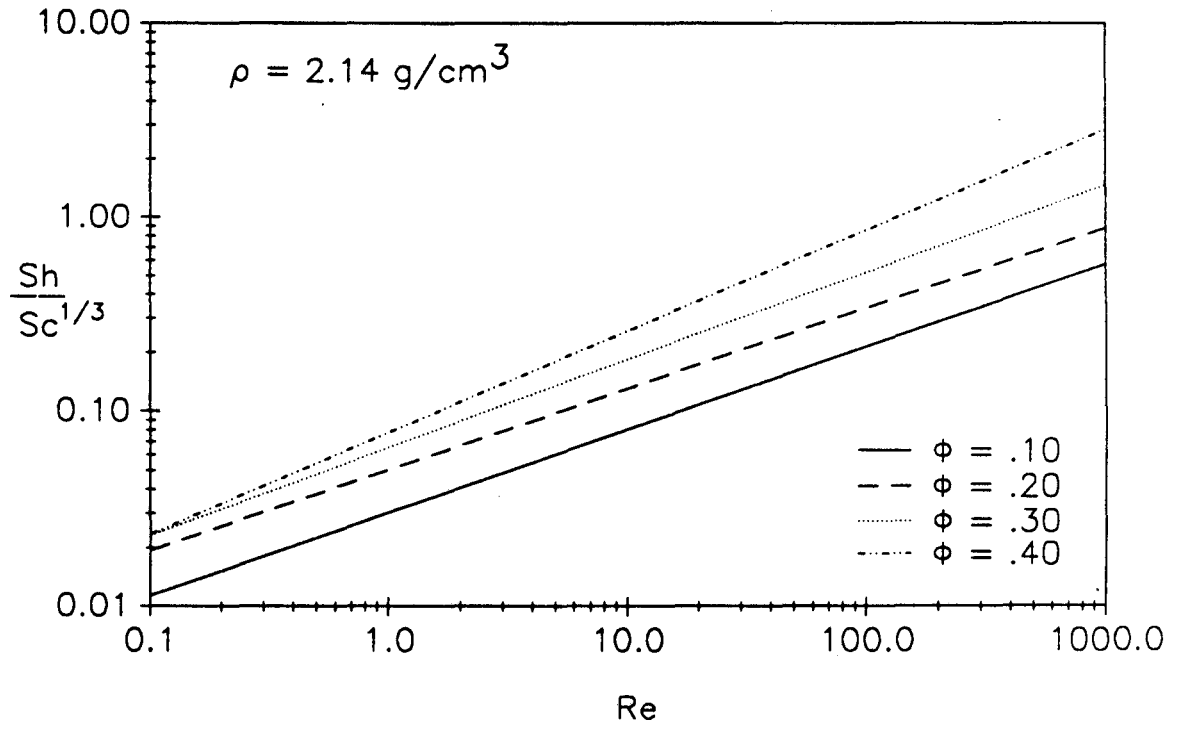
XBL 9011-3811

Figure 13



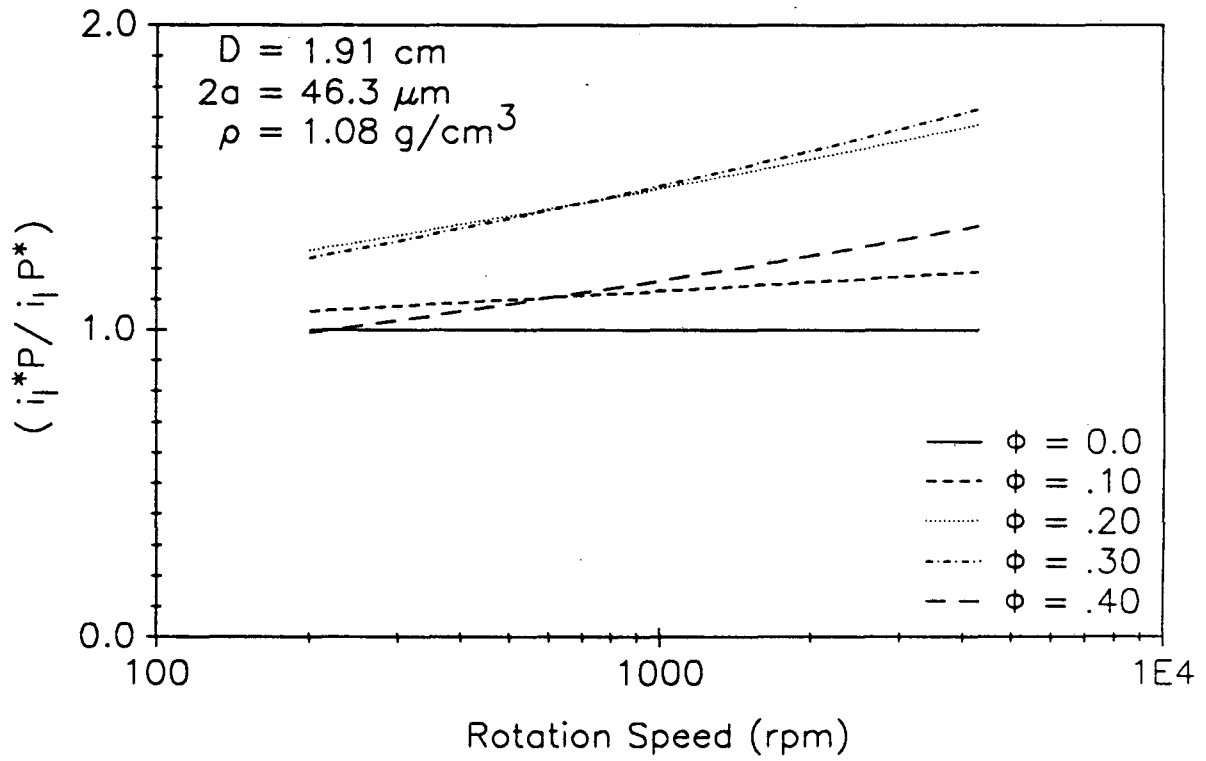
XBL 9011-3812

Figure 14



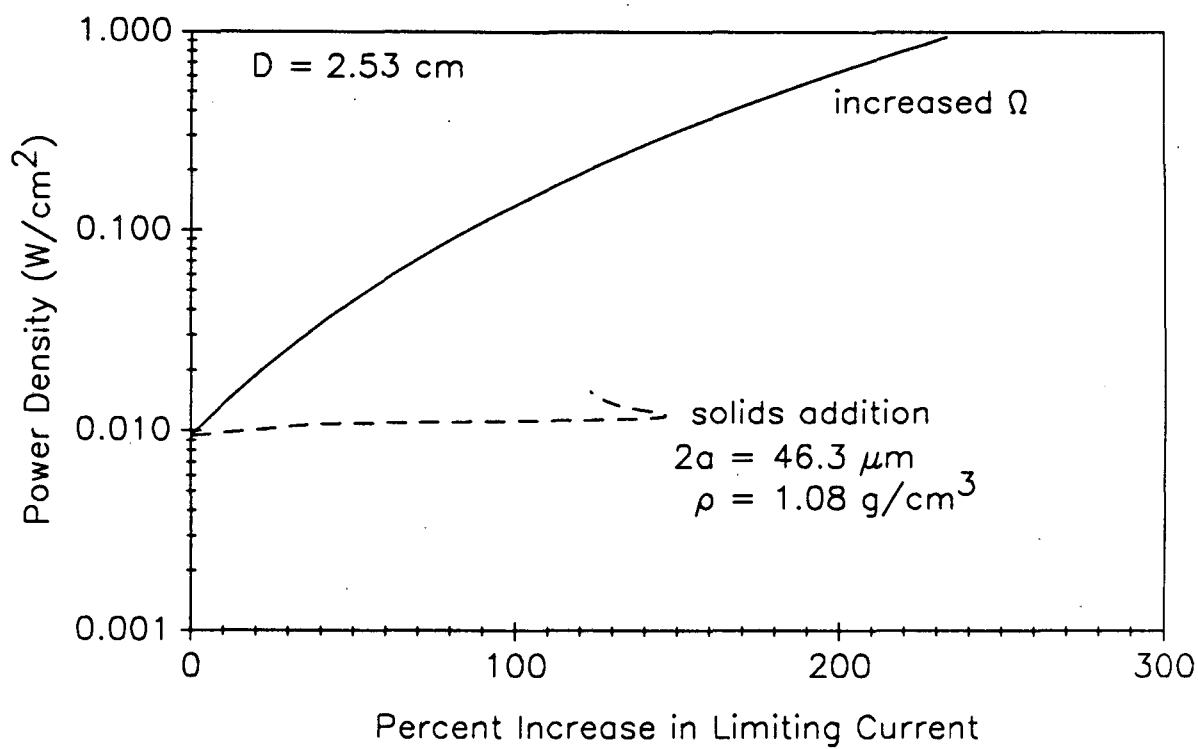
XBL 9011-3813

Figure 15



XBL 9011-3817

Figure 16



XBL 9011-3818

Figure 17

LAWRENCE BERKELEY LABORATORY  
UNIVERSITY OF CALIFORNIA  
INFORMATION RESOURCES DEPARTMENT  
BERKELEY, CALIFORNIA 94720